COPPE
Instituto Alberto Luiz Coimbra de Pós-Graduação e Pesquisa de Engenharia
UFRJ

ON THE CONTRIBUTION OF POWER CONVERTERS AND SYNCHRONOUS GENERATORS TO SHORT-TERM VOLTAGE STABILITY: A COMPARATIVE ANALYSIS

Marcos Jorge Araujo de Souza

Dissertação de Mestrado apresentada ao Programa de Pós-graduação em Engenharia Elétrica, COPPE, da Universidade Federal do Rio de Janeiro, como parte dos requisitos necessários à obtenção do título de Mestre em Engenharia Elétrica.

Orientadores: Luís Guilherme Barbosa Rolim
Thiago José Masseran Antunes Parreiras

Rio de Janeiro
Novembro de 2023

ON THE CONTRIBUTION OF POWER CONVERTERS AND SYNCHRONOUS GENERATORS TO SHORT-TERM VOLTAGE STABILITY: A COMPARATIVE ANALYSIS

Marcos Jorge Araujo de Souza

DISSERTAÇÃO SUBMETIDA AO CORPO DOCENTE DO INSTITUTO ALBERTO LUIZ COIMBRA DE PÓS-GRADUAÇÃO E PESQUISA DE ENGENHARIA DA UNIVERSIDADE FEDERAL DO RIO DE JANEIRO COMO PARTE DOS REQUISITOS NECESSÁRIOS PARA A OBTENÇÃO DO GRAU DE MESTRE EM CIÊNCIAS EM ENGENHARIA ELÉTRICA.

Orientadores: Luís Guilherme Barbosa Rolim
Thiago José Masseran Antunes Parreiras

Aprovada por: Prof. Luís Guilherme Barbosa Rolim, Dr.-Ing.
Prof. Thiago José Masseran Antunes Parreiras, D.Sc
Prof. Thiago Cardoso Tricarico, D.Sc.
Prof. João Alberto Passos Filho, D.Sc.

RIO DE JANEIRO, RJ – BRASIL
NOVEMBRO DE 2023

Souza, Marcos Jorge Araujo de

On the contribution of power converters and synchronous generators to short-term voltage stability: a comparative analysis/Marcos Jorge Araujo de Souza. – Rio de Janeiro: UFRJ/COPPE, 2023.

XX, 74 p.: il.; 29, 7cm.

Orientadores: Luís Guilherme Barbosa Rolim

Thiago José Masseran Antunes Parreiras

Dissertação (mestrado) – UFRJ/COPPE/Programa de Engenharia Elétrica, 2023.

Referências Bibliográficas: p. 66 – 70.

1. Short-term voltage stability. 2. Synchronverter. 3. Saddle-node bifurcation. 4. Short-term voltage stability enhancement. I. Rolim, Luís Guilherme Barbosa *et al.* II. Universidade Federal do Rio de Janeiro, COPPE, Programa de Engenharia Elétrica. III. Título.

"A discriminação dos negros está presente em cada momento das suas vidas para lembrá-los que a inferioridade é uma mentira que só aceita como verdadeira a sociedade que os domina."
Martin Luther King

Agradecimentos

Em primeiro lugar gostaria de agradecer a amigos e familiares, em particular aos meus pais: Elisangela de Araujo Souza Mourão e Marcos Salvador de Souza, por todo amor e carinho.

Agradeço também à UFRJ e em especial aos funcionários que nela trabalham, por sua dedicação em tornar esta universidade plural e uma referência acadêmica.

Agradeço também aos colegas de trabalho da Jordão por todo o aprendizado recebido que será de grande valia para o meu futuro profissional.

Aos membros da banca agradeço por se disponibilizarem a avaliar meu trabalho, os pontos destacados serão de grande relevância para a versão final deste trabalho. Em particular, agradeço aos meu orientadores: Luís Guilherme Barbosa Rolim e Thiago José Masseran Antunes Parreiras, os quais assumiram a minha orientação após o falecimento precoce do professor Maurício Aredes, o qual me orientou na graduação, iniciou a minha orientação de mestrado e me ajudou a desenvolver meu interesse por pesquisa, muito obrigado.

Resumo da Dissertação apresentada à COPPE/UFRJ como parte dos requisitos necessários para a obtenção do grau de Mestre em Ciências (M.Sc.)

ON THE CONTRIBUTION OF POWER CONVERTERS AND SYNCHRONOUS GENERATORS TO SHORT-TERM VOLTAGE STABILITY: A COMPARATIVE ANALYSIS

Marcos Jorge Araujo de Souza

Novembro/2023

Orientadores: Luís Guilherme Barbosa Rolim
Thiago José Masseran Antunes Parreiras

Programa: Engenharia Elétrica

A entrada massiva de fontes de energia renováveis no sistema elétrico aumenta o número de conversores de energia conectados à rede, antes dominada por máquinas síncronas. Além disso, para melhorar a operação do sistema de energia, muitos dispositivos baseados em eletrônica de potência também são conectados à rede, como HVDC, STATCOM, entre outros. Isso levanta questões sobre como essa mudança de paradigma nos sistemas elétricos de potência pode afetar a estabilidade do sistema.

Na literatura, muitas estratégias de controle para conversores são continuamente apresentadas, pois, diferentemente das máquinas síncronas, sua dinâmica depende de um modelo matemático que pode ser apresentado de diversas formas.

Além disso, com o aumento contínuo do consumo de energia elétrica, novas cargas são continuamente conectadas ao sistema, sejam motores de indução tradicionais, com baixa inércia, como é o caso dos modernos ar condicionados, ou cargas eletrônicas com dinâmicas que podem interagir adversamente com o sistema de energia, especialmente em relação à estabilidade de tensão de curto prazo.

Portanto, esta dissertação pretende apresentar uma comparação de algumas estratégias de controle de conversores e seu desempenho frente a eventos que podem levar a instabilidade de tensão de curto prazo. Também será apresentada uma variação do tempo de subida das malhas de potência ativa e tensão no controle em referência *dq*. Serão propostas alterações no controle do *Synchronverter* e será feita uma comparação com o modelo tradicional para avaliar o desempenho. Simulações em PSCAD serão realizadas para apresentar as análises.

Abstract of Dissertation presented to COPPE/UFRJ as a partial fulfillment of the requirements for the degree of Master of Science (M.Sc.)

ON THE CONTRIBUTION OF POWER CONVERTERS AND SYNCHRONOUS GENERATORS TO SHORT-TERM VOLTAGE STABILITY: A COMPARATIVE ANALYSIS

Marcos Jorge Araujo de Souza

November/2023

Advisors: Luís Guilherme Barbosa Rolim
Thiago José Masseran Antunes Parreiras

Department: Electrical Engineering

The massive entry of renewable energy sources into the power system increases the number of power converters connected to the grid, previously dominated by synchronous machines. Furthermore, to improve the operation of the power system, many devices based on power electronics are also connected to the grid, such as HVDC, and STATCOM, among others. This raises questions about how this paradigm shift in electrical power systems might affect system stability.

In the literature, many control strategies for converters are continuously presented, since, unlike synchronous machines, their dynamics depend on a mathematical model that can be presented differently.

Furthermore, with the continuous increase in electricity consumption, new loads are continuously connected to the system, whether traditional induction motors, with low inertia, as in the case of modern air conditioning, or electronic loads with dynamics that can adversely interact with the power system, especially regarding short-term voltage stability.

Therefore, this dissertation intends to compare some converter control strategies and their performance against events that can lead to short-term voltage instability. A rise time variation of the active power and voltage in the control in dq-Frame will also be presented. Changes in the synchronverter control will be proposed and a comparison with the traditional model will be made to evaluate the performance. PSCAD simulations will be performed to present the analysis.

Contents

List of Figures

List of Tables

List of Symbols

C_d	Damping Capacitor, p. 36
C_f	Filter Capacitor, p. 36
H	Inertia constant, p. 46
I_{max}	Maximum supported current by the converter, p. 39
J	Moment of Inertia, p. 36
J_v	Synchronverter's virtual inertia, p. 44
L_1	Inductance converter-side, p. 36
L_2	Inductance grid-side, p. 36
L_m	Magnetizing Inductance, p. 36
L_r	Rotor Leakage Inductance, p. 36
L_s	Stator Leakage Inductance , p. 36
R_1	Resistance converter-side, p. 36
R_2	Resistance grid-side, p. 36
R_a	Armature resistance, p. 46
R_d	Damping resistance, p. 36
R_r	Rotor resistance, p. 36
R_s	Stator resistance, p. 36
S_{im}	Induction motor rated power, p. 36
T''_d	d-axis sub-transient time constant, p. 46
T''_q	q-axis sub-transient time constant, p. 46

T'_d — d-axis transient time constant, p. 46

T_d — Synchronverter's Droop Torque, p. 44

T_e — Electromagnetic Torque, p. 29

T_e^{sync} — Synchronverter's Electromagnetic Torque, p. 44

T_{ref} — Synchronverter's Mechanical Torque Reference, p. 44

V_{ll} — Line to line voltage, p. 46

ψ_v — Synchronverter's virtual flux, p. 45

b_c — Capacitor susceptance, p. 35

$g_{Static\ Load}$ — Static Load conductance, p. 35

$i^{**}_{\alpha p}$ — Active α-current reference after limiter, p. 40

$i^{*}_{\alpha p}$ — Active α-current reference before limiter, p. 40

$i^{**}_{\alpha q}$ — Reactive α-current reference after limiter, p. 40

$i^{*}_{\alpha q}$ — Reactive α-current reference before limiter, p. 40

$i^{**}_{\beta p}$ — Active β-current reference after limiter, p. 40

$i^{*}_{\beta p}$ — Active β-current reference before limiter, p. 40

$i^{**}_{\beta q}$ — Reactive β-current reference after limiter, p. 40

$i^{*}_{\beta q}$ — Reactive β-current reference before limiter, p. 40

i_{conv} — Current converter-side, p. 36

i^{**}_d — d-current reference after limiter, p. 38

i^{*}_d — d-current reference before limiter, p. 38

i_{grid} — Current grid-side, p. 36

i^{**}_q — q-current reference after limiter, p. 38

i^{*}_q — q-current reference before limiter, p. 38

$k_i^{apl-\alpha\beta}$ — Active power loop integral gain of the control in $\alpha\beta$-Frame, p. 40

k_i^{apl-dq}	Active power loop integral gain of the control in dq-Frame, p. 38
k_i^{cl}	Vectorial control current loop integral gain, p. 38
k_i^{pll}	SRF-PLL integral gain, p. 37
$k_i^{vl-\alpha\beta}$	Voltage loop integral gain of the control in $\alpha\beta$-Frame, p. 40
k_i^{vl-dq}	Voltage loop integral gain of the control in dq-Frame, p. 38
$k_p^{apl-\alpha\beta}$	Active power loop proportional gain of the control in $\alpha\beta$-Frame, p. 40
k_p^{apl-dq}	Active power loop proportional gain of the control in dq-Frame, p. 38
k_p^{cl}	Vectorial control current loop proportional gain, p. 38
k_p^{pll}	SRF-PLL proportional gain, p. 37
$k_p^{vl-\alpha\beta}$	Voltage loop proportional gain of the control in $\alpha\beta$-Frame, p. 40
k_p^{vl-dq}	Voltage loop proportional gain of the control in dq-Frame, p. 38
x_d''	d-axis sub-transient reactance, p. 46
x_q''	q-axis sub-transient reactance, p. 46
x_d'	d-axis transient reactance, p. 46
x_d	d-axis reactance, p. 46
x_p	Potier reactance, p. 46
x_q	q-axis reactance, p. 46

List of Abbreviations

ANEEL	Agência Nacional de Energia Elétrica, Brazilian National Electric Energy Agency, p. 1
AVR	Automatic Voltage Regulator, p. 12
BIPS	Brazilian Interconnected Power System, p. 1
CCT	Critical clearance time, p. 32
CSII	Converter-Driven Slow Interaction Instability, p. 21
DVS	Dynamic voltage support, p. 31
EPE	Empresa de Pesquisa Energética, Brazilian Energy Research Company, p. 1
EPS	Electrical Power System, p. 1
ERAC	Esquema Regional de Alívio de Carga, Brazilian Regional Load Relief Scheme, p. 13
ESS	Energy Storage System, p. 1
FACTS	Flexible AC Transmission Systems, p. 1
FIDVR	Fault-induced Delayed Voltage Recovery, p. 21
FRT	Fault Ride Through, p. 7
GOV	Speed Governors, p. 12
HVDC	High Voltage Direct Current, p. 1
IM	Induction motor, p. 13
LCC	Line-Commutated Converter, p. 28
LCL	Inductor-Capacitor-Inductor filter, p. 36

LTM1	Long-term voltage stability mechanism one, p. 24
LTM2	Long-term voltage stability mechanism two, p. 25
LTM3	Long-term voltage stability mechanism three, p. 25
LTVI	Long-term Voltage Instability, p. 24
LTVS	Long-Term Voltage Stability, p. 21
OEL	Over-Excitation Limiter, p. 46
OLTC	On Load Tap Changer, p. 24
ONS	Operador Nacional do Sistema Elétrico, Brazilian Power System Operator, p. 9
PCC	Point of Common Coupling, p. 9
PDE	Plano decenal de expansão de energia, Brazilian Ten-Year Energy Expansion Plan, p. 1
PI	Proportional Integral, p. 37
PMU	Phasor Measurement Units, p. 14
PR	Proportional Resonant, p. 40
PSCAD™/EMTDC™	Power Systems Computer-Aided Design/Electromagnetic Transients including DC, p. 18
PSS	Power system stabilizer, p. 12
PV-plane	Active power versus bus voltage, p. 13
RES	Renewable Energy Source, p. 1
S-LTM1	STVS induced by LTVS mechanism one, p. 25
S-LTM2	STVS induced by LTVS mechanism two, p. 25
S-LTM3	STVS induced by LTVS mechanism three, p. 25
SRF-PLL	Synchronous reference frame - Phase-locked loop, p. 37
STM1	Short-term voltage stability mechanism one, p. 22
STM2	Short-term voltage stability mechanism two, p. 22
STM3	Short-term voltage stability mechanism three, p. 22

STVI	Short-Term Voltage Instability, p. 2
STVS	Short-Term Voltage Stability, p. 15
SVC	Static Var Compensators, p. 30
TRAI	Transient Rotor Angle Instability, p. 4
TVSR	Transient Voltage Stability Ratio, p. 14
VSC	Voltage Source Converter, p. 16
ZIP	ZIP load model, p. 12

Chapter 1

Introduction

1.1 Contextualization

The demand to decrease carbon launch into the atmosphere has been leading to increasing penetration of renewable energy sources (RES) in the power system, provoking a change in the traditional system structure.

Moreover, Flexible AC Transmission Systems (FACTS), High Voltage Direct Current (HVDC), and power electronics interfaced loads have also been increasing across the world. Solar photovoltaic, wind energy, and energy storage systems (ESS) are connected to the Electrical Power System (EPS) through a power electronics converter, which brings new types of instability to the system [1], and make the previous instability mechanisms more complex, for instance, the EPS has been facing:

- Inertia reduction, which affects the frequency stability of the EPS;
- Adverse interaction between HVDC, known as multi-infeed interaction;
- Among others.

The Brazilian Energy Research Company (EPE) publishes every year a study indicating the perspectives of the expansion of the Brazilian Interconnected Power System (BIPS) for the next ten years in the document called Brazilian Ten-Year Energy Expansion Plan (PDE).

According to the PDE, 2032 [2], there will be a massive entry of RES in the next years, especially in the North and North East of the BIPS. For 2025, it is counted 34 GW of wind and solar photovoltaic energy hired or confirmed. In the Brazilian National Electric Energy Agency (ANEEL) database [3] it is possible to see details on the power plants to enter in the BIPS for the next years.

The worldwide trend is for an increase in energy consumption. In the BIPS, according to reference [4], an increase of 3.6% in the load demand per year is predicted. Furthermore, with the massive entry of renewable energy into the BIPS, it is more viable to transmit the energy via HVDC links to the main customer center, South and South East of BIPS, increasing the operational complexity of the Brazilian power System. This global tendency might affect the stability margin of power systems in general.

1.2 Objectives

For a secure and reliable power system operation, it is necessary to understand the solution techniques of the instability mechanisms. Regarding voltage stability, the literature focuses more on long-term instability. At the same time, the short-term has been neglected over other short-term instabilities like frequency and angular instability [5].

Hence, this dissertation aims to expand the existing literature on short-term voltage instability (STVI) considering the increasing of IBGs in the EPS. Thus contributing to the understanding of the performance of the power converter regarding STVI. Moreover, the power converter embedded with its control strategies will be compared to the synchronous generator, the traditional power plant in the power system.

Therefore, to achieve this goal, three specific goals are proposed for this dissertation:

- Comparative analysis between power converters control and synchronous machine:

  It is known that the control strategy influences the stability of the EPS. Regarding power converters, it is possible to find loads of control strategies in the literature with different characteristics and purposes. This raises the question of how those control strategies interact with the STVI. Therefore, this dissertation will conduct a comparative analysis using some control strategies for power converters: control in dq-Frame, control in $\alpha\beta$-Frame, and synchronverter control, a synchronous generator will also be compared. As the traditional power system is composed of synchronous machines, comparing them to a power converter is necessary to understand the difference in performance regarding STVI events. To enable a fair comparison, all the controllers will be designed based on the rise time parameter.

- Analysis of the rise time variation of the outer loop of the control in dq-Frame impacts on STVI:

The dynamic behavior of a power converter is dominated by its control strategy and depends on the performance parameters designed like settling time, rise time, and others. The controllers were designed for this dissertation based on the rise time parameters. An analysis varying this parameter will be conducted in the control in *dq*-Frame to verify its influence on STVI.

- Change in the synchronverter structure and analysis of its impact on STVI:

  The synchronverter is a control strategy that aims to mimic a synchronous machine as presented in [6]. In this dissertation, a change in the virtual flux loop generator will be proposed to improve its performance in the case of STVI events, and the analysis in the test network will be presented to validate the proposal.

1.3 Case Study Structure

Figure 1.1 shows the radial power system employed for the analysis. This system is based on the power system presented in [7]. Two lines were added between buses 2 and 3 to enable contingency analysis evaluating one of the STVI mechanisms. In addition, the local generation was moved to bus 5 to enable a more realistic analysis, as long as in actual power systems, the load is not in the same bus as the power plant.

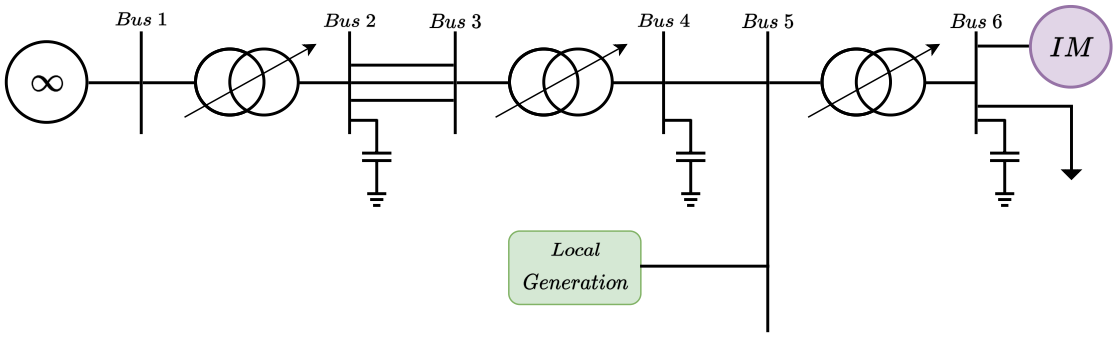

Figure 1.1: Power system used for the analysis.

This system was chosen because it is simple and appropriate for analysis as the STVI phenomenon is observable [7]. However, [8] proposes a benchmark for studies related to voltage stability. Nonetheless, this system was not chosen as it is normally used for LTVI studies, and its bigger size is unsuitable for the proposed analysis. In [9], there are also more example systems with similar characteristics of the system in Figure 1.1.

1.4 Methodology

For the three analyses proposed in this dissertation, a PSCAD simulation will be performed. The power system proposed in the reference [7] shown in Figure 1.1 will be modeled in PSCAD with the parameters changed as presented in Chapter 4 along with the controllers also presented in Chapter 4.

To enable a fair comparison between the controllers, it is proposed to design the gains considering the rise time of the outer loop as a reference. The design procedure is presented in the Appendix A.

Short-circuit and impedance variation will be applied in the power system for the analysis described in chapter 5. These events are known to cause voltage collapse in the power which is the focus of this work, although oscillatory instability is also a type of STVI it will not be addressed in this dissertation. For each study case, three metrics will be considered:

- Transient voltage performance analysis:
  - This metric aims to analyze the performance dynamic behavior of the system after a disturbance regarding the compensator design and control.
- Critical clearance time (CCT) of a short circuit measurement:
  - The CCT is a well-known metric for Transient Rotor Angle Instability (TRAI). This metric captures the region of attraction to the system's equilibrium and will be used as a metric for the STVI region of attraction.
- Saddle-node stability margin measurement:
  - The Saddle-node bifurcation is well-known for LTVI assessment. This metric captures the maximum capacity of the system to transmit power across an inductive network. In this dissertation, the load and the local generator's dynamic will be considered to identify the point of voltage collapse.

1.5 Document Structure

After the introduction, chapter 2 presents stability concepts and existing research, chapter 3 presents theoretical foundations on voltage stability focusing on the short-term time frame, chapter 4 presents the case study structure along with the equipment and their controllers, chapter 5 presents the methodology, chapter 6 presents the results and discussion, finally, chapter 7 conclude this work.

Chapter 2

Problem Definition and Literature Review

2.1 Power System Stability Problem and Definitions

Power system stability is an important topic in electrical engineering. Through stability assessment, it is possible to ensure a secure and stable operation of the power system. The formal definition of power system stability is given in [10]: the power system is said to be stable for a certain operating point if, after being subjected to a disturbance, the system can reach the same or another stable operating point.

The stability of power systems is similar to the stability of any dynamic system. However, this kind of system is highly nonlinear and operates in constant change of its structure for different time horizons, short or long. The stability properties will depend on different aspects, such as the nature of the disturbance, whether it is small or large, the equilibrium point, network topology, and others.

The stability concept of power systems was updated as presented in [1]. Figure 2.1 shows a diagram illustrating the different types of stability. The new definition and classification were due to the increase of power electronics devices connected to the grid, such as HVDC, FACTS, wind farms, and photovoltaic generation.

For the classical classification (rotor angle, voltage, and frequency stability) of power system stability, the assessment can be made by phasor (or quasi-sinusoidal) approximation. Nonetheless, for the new types of power system stability classification (resonance and converter-driven stability), this approximation type can not be used effectively for every study. Nevertheless, in the case of voltage stability, the definitions remain the same, except that the effects of HVDC were included in the short-term voltage stability.

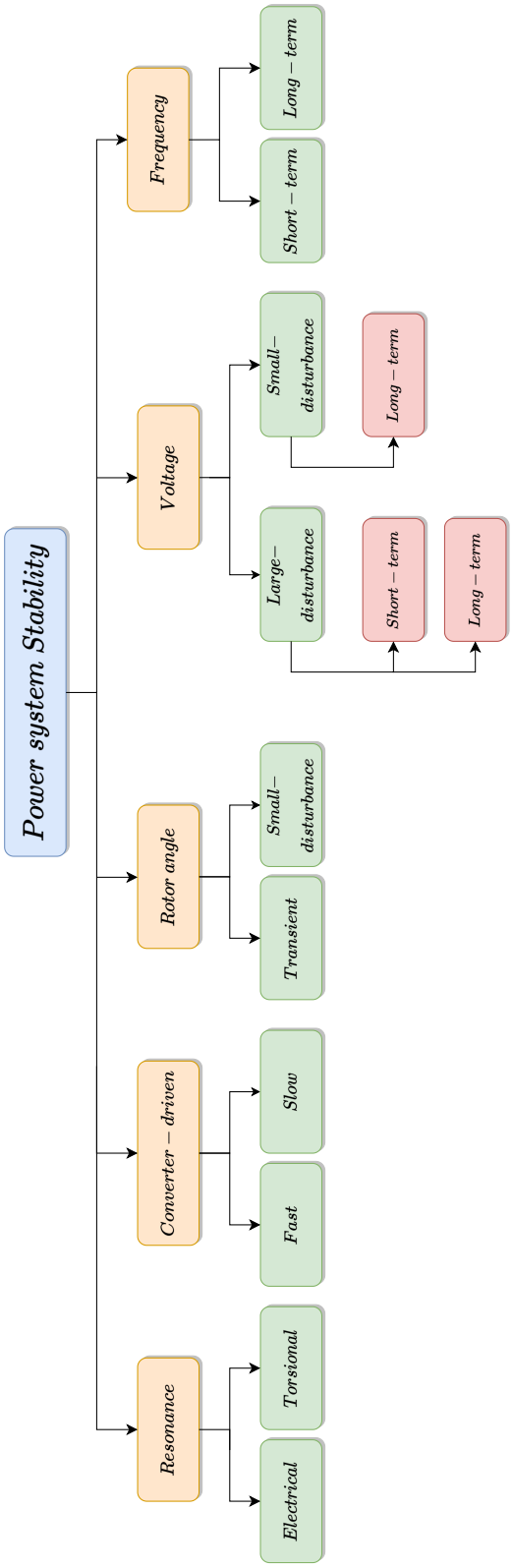

Figure 2.1: Stability definition.

2.2 Short-Term Voltage Instability Real Incidents

Some real incidents were caused by voltage instability reported in the literature [9, 11–13]. In this section, only short-time incidents will be presented[1]:

- Czechoslovakia, 1985 [11]:

  The strong part of the system got disconnected from the weak and loaded part of the system because of outages of large sources, leading to a fast voltage collapse and loss of synchronism.

- South Florida, USA, 1985 [9]:

  After a fire, three lightly loaded lines tripped, resulting in a blackout. For this case, some transient simulations were performed. The result indicated that the system should have recovered. This case raised suspicion about load modeling.

- Nelson River HVDC system, Canada, 1986 [9]:

  Voltage collapse occurred during the energizing of a transformer, leading to commutation failure and voltage collapse.

- Itaipu HVDC link, Brazil, 1986 [9]:

  After many equipment outages, the AC voltage close to the inverter substation dropped, leading to successive commutation failure and load shedding. This disturbance and others led to changes in the DC control system.

- Western Tennessee, USA, 1987 [9]:

  A large short circuit resulted in a voltage depression of values between 0.75 *pu* and 0.82 *pu* in the 500 kV and 161 kV systems for approximately 10 seconds after the fault clearing. The motors connected to the grid increased their reactive power demand, contributing to voltage collapse. This event caused a load loss of 1.265 GW.

- Great Britain, 2019 [12, 14]:

  A blackout happened in the United Kingdom (UK) system after a fault caused by incorrect adjustments in a ride-through setting of power converters. In [15], the impact of fault ride-through (FRT) in STVI is explained.

References [16, 17] discuss previous blackouts that have occurred in power systems across the world. Most of them were related to voltage instability. In [17],

[1] Short-term voltage instability real events between 1987 and 2019 were not found by the author of this dissertation.

the events start from 1965 while in [16] the focus is on the events from 2003 to 2015. However, in these references, it is unclear if the blackout happened because of long-term or short-term voltage instability. This way, the events reported were not included in the above list.

2.3 Analysis Methodology

Voltage stability is a complex phenomenon to analyze. There are different methodologies of analysis in the literature. This section will present the methods according to the computational burden as presented in [18].

- Static methods:

  Power system instability is a dynamic phenomenon. However, some static methods can be used to assess voltage stability. The statics methods are used to determine the condition of the power system for steady-state situations, or the power flow might be used to measure the maximum deliverable power of such a system and determine the stability margin.

- Time scale decomposition methods:

  The time scale decomposition aims to capture the main variables to asses the voltage instability. For short-term instability, the fast variables are modeled by a dynamic equation, while the slow variables are modeled by algebraic equations. In the case of long-term instability, it is the opposite. The short-term dynamics are considered to be stable and modeled by the equilibrium equation.

- Dynamic methods:

  Nonlinear time-domain simulation is capable of evaluating both short-term and long-term simulations once the modeling of the components represents better the power system. The disadvantage is the higher computational burden compared to others.

Artificial intelligence techniques have gained space in much research recently as the development of these techniques and the computational processing capability, make them suitable to analyze nonlinear systems such as the power system. Reference [19] presents a review of analysis methods to assess power system transient stability, focusing on artificial intelligence techniques. The techniques include machine learning, deep learning, and enforcement learning.

2.4 Brazilian Grid Code

In Brazil, the guidelines for power systems operations are defined by the Brazilian Power System Operator (ONS). ONS is responsible for operating the system at voltages above 230 kV. In the BIPS, these voltage levels are 230, 345, 440, 500/525, 600, 750, and 800 kV, according to the reference [20]. The most relevant aspects regarding voltage stability and the continuous operation of power converters will be presented in this section.

The Brazilian grid code document [21] presents the minimal technical requirements for the connection of equipment to the power transmission system in Brazil. Its main aspects will be presented in Section 2.4.1. The modeling criteria and methodology to perform electrical study are given by the technical document [22], whose main aspects regarding voltage stability modeling requirements will be presented in Section 2.4.2, while the premises for voltage stability assessment will be presented in Section 2.4.3.

2.4.1 Operation of Power Converters Connected to the Brazilian Grid

System Operation Under Fault

In the case of the power system being subjected to voltage fluctuations in one or more phases, regardless of the disturbance, the requirements for power converters, photovoltaic, and wind energy, to operate without disconnection from the grid is shown in Figure 2.2. This characteristic must be attended by the phase that suffers the biggest variation on the point of common coupling (PCC), and it is known as voltage ride-through.

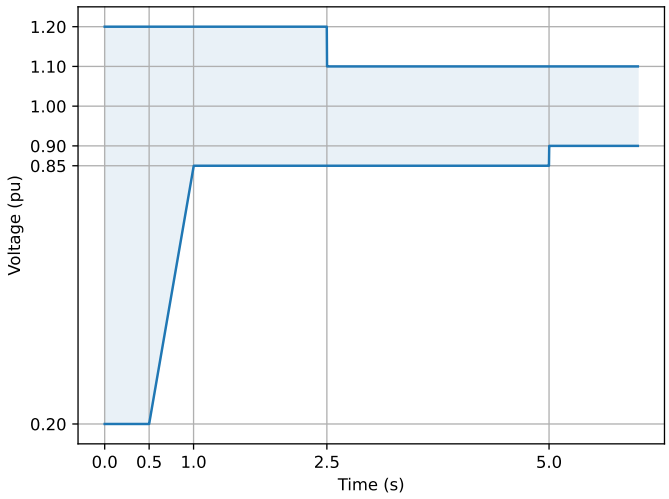

Figure 2.2: Voltage ride-through requirements in the BIPS.

Figure 2.3 shows how the power converter must act in case of transient voltage variations at the PCC. In the case of under voltage, the converters must provide additional reactive power to the system. In the case of overvoltage, the power converter must absorb additional reactive power. The range of non-operation varies from 0.85 *pu* to 1.1 *pu*. In case a voltage goes beyond this interval, the power converter must help the system control its voltage. The slope θ will be given according to ONS instructions.

The variation of reactive current is defined as:

$$\Delta I_q = I_q - I_{q0} \tag{2.1}$$

where,

- I_q is the reactive current, measured from the converter to the grid direction
- I_{q0} is the pre-disturbance reactive current

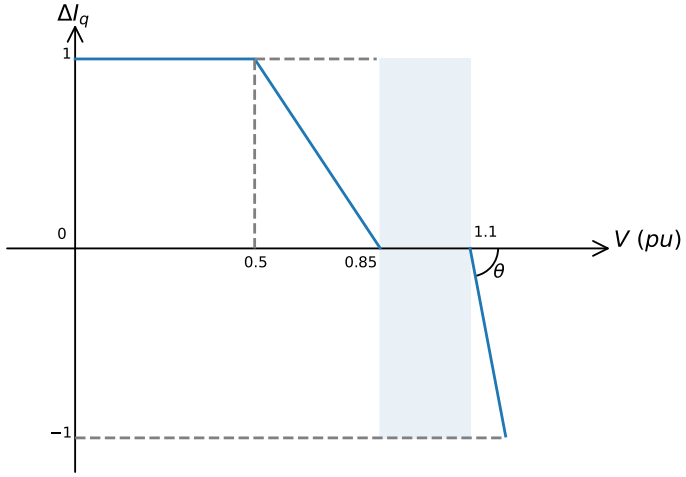

Figure 2.3: Reactive current requirements under fault.

General Requirements for Steady-State Operation

The RES connected to the BIPS must be able to operate in three types of control: voltage control, reactive power control, and constant power factor control.

The main control mode operation is the voltage control, and the voltage profile characteristic is shown in Figure 2.4. The reference voltage is adjustable between 0.95 *pu* and 1.05 *pu*, and the slope must be adjustable between 2% and 7%.

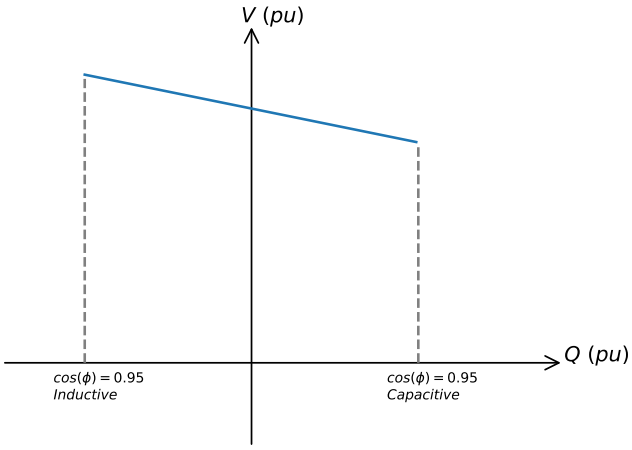

Figure 2.4: Voltage profile control in the voltage control mode of the RES.

The reactive power of the RES, when operating in the constant power factor mode and in the presence of non-nominal voltage, should meet the specified requirements illustrated in Figure 2.5. P_{max} is the lowest value between the hired active power and the available active power summation of all installed generated units.

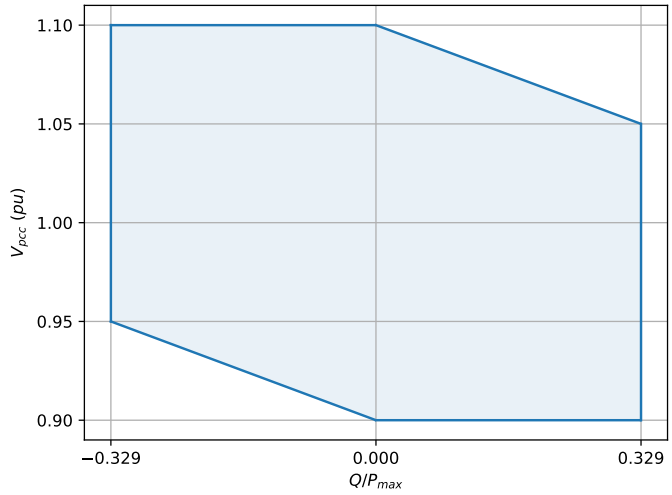

Figure 2.5: Reactive power versus voltage requirements in the constant power factor operation mode.

In a steady state, the RES must be able to operate in the region shown in Figure 2.6 even in the case of low active power production.

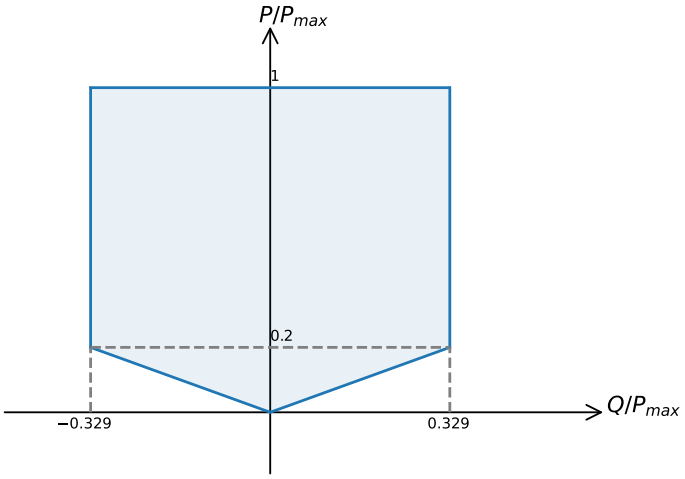

Figure 2.6: Steady state operation requirements for power converter connected to the BIPS.

2.4.2 Modeling Requirements

Static Analysis

The modeling premises for static analysis are:

- Loads should be represented as constant power, however, the ZIP model can be used for specific purposes;
- Specific loads like aluminum industry or large induction motors can be represented by detailed models, such as dynamic models.

Dynamic Analysis

In the case of dynamic analysis, the modeling requirements are:

- Synchronous generator:
  - Thermal generators must be modeled by round rotor including saturation and damper windings;
  - Hydro generators must be represented by salient poles including saturation and damper windings;
  - Automatic Voltage Regulator (AVR), speed governors (GOV), and Power system stabilizer (PSS) must be modeled for each machine modeled if the machine has the control installed;
  - Limiters and devices that affect the PSS generator must be modeled.
- Loads must be modeled in the most realistic way possible whether static or dynamic, linear or not, depending on the available data;

- HVDC links must be also represented according to the premises in [22];
- FACTS devices must be represented with their control;
- Photovoltaic and wind turbine power plants must be represented if their loop control acts on the same time scale as the electromechanical analysis;
- Load shedding schemes such as Brazilian Regional Load Relief Scheme (ERAC) must be represented if relevant to the analysis.
- Induction motor (IM) must be represented by a detailed dynamic model, in case it is not possible, the active power of the motor must be represented by constant current and the reactive power by constant impedance.

2.4.3 Voltage Stability Assessment in Brazil

Dynamic Overvoltage Assessment

Dynamic overvoltage is another type of voltage instability, it might be caused by no-load energizing of long lines, and load rejection by long lines, among others. For this type of study, ONS recommends modeling the long lines by frequency-dependent models.

The simulation must run for at least 8 seconds, in which the overvoltages are observed and plotted in a graph as a function of the generator speed. In case of load rejection, the worst system contingency, a non-operation of one or more equipment in the system, should also be considered.

Voltage Security Assessment

The voltage security margin is defined as the minimal distance[2] to an operation point where there is a risk of voltage instability. It is recommended to have at least a 4% margin in real-time operation [22].

To assess the voltage security of the BIPS, both dynamic and static analysis can be done, but the dynamic must agree with the static one. In the case of static analysis, it is recommended that the power factor be kept constant for the whole process. The re-dispatch chosen is the one that achieves the critical load in the system by increasing or decreasing the power dispatch of the generators needed to achieve this critical operation point.

[2]In the technical document, it is not explained how this distance is measured, but usually, it is made by using the PV-plane

2.5 Voltage Stability Indices

2.5.1 Prediction and Prevention Indices

Reference [23] presents an overview of voltage stability indices. The voltage stability index is used to measure how far is the system to the instability point. They can be used to predict instability and apply corrective actions to avoid it. The types of preventive and predictive indices found in the literature, classified according to reference [23] are:

- Based on system parameters:

  This class of indices uses the system parameters to estimate the voltage stability margin the parameters used include:

  - Bus parameters based;
  - Line parameters based;
  - Based on Jacobian matrix;

- Based on phasor measurement units (PMU):

  The methods based on PMU are usually used for real-time assessments and they are divided into:

  - Load measurement;
  - Observability.

The methods above have their advantages and disadvantages. According to [23] the performance of each index depends on the network operation.

2.5.2 Transient Behavior Performance Evaluation Index

References [24, 25] discuss the location and type of a reactive power device based on an index that evaluates the performance of a power system after being subjected to a fault. The index presented in reference [25] will be used in this dissertation and will be explained in detail in this section.

The transient voltage stability ratio (TVSR) index aims to analyze the voltage behavior in terms of damping and how fast the compensator device brings the voltage back to the pre-fault value. The ideal scenario is shown in Figure 2.7a, which consists of the voltage recovering itself immediately after the fault is clear. A common scenario is a case shown in Figure 2.7b, where the voltage takes more time to reach the pre-fault value. In this non-ideal scenario, there are two areas A_1 and A_2, that represent how the transient voltage deviates from the ideal scenario.

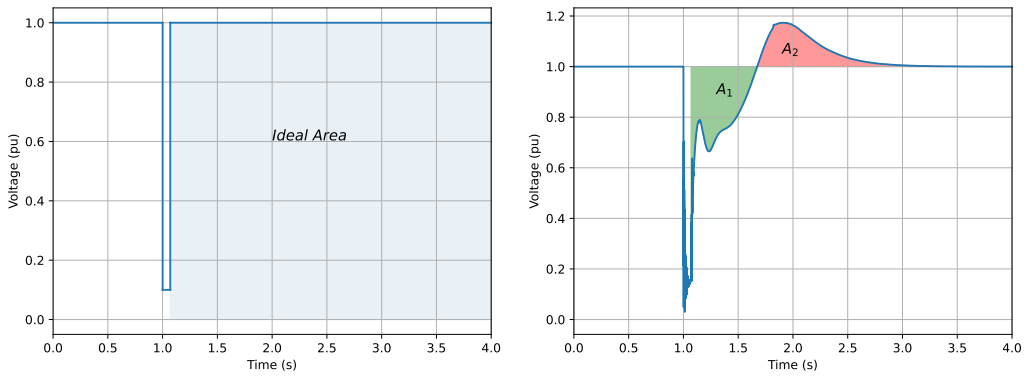

(a) (b)

Figure 2.7: Dynamic voltage transient (a) ideal and (b) typical.

The TVSR index is calculated by comparing both ideal and non-ideal transients as in the formula:

$$TVSR(\%) = 100 \times \frac{A_1 + A_2}{Ideal\ Area} \tag{2.2}$$

In the ideal scenario, the TVSR is zero, therefore as lower the TVSR is better the system behavior.

The TVSR metric counts both A_1 and A_2 areas with the same importance to determine how the voltage deviates from the ideal, in some cases a fast recovery of the voltage might be more important for the system than the overshoot, as long as the maximum value is acceptable according to the grid code.

Moreover, the reference [25] does not stabilize a rule to define the time window, if it is too large the ideal area makes the TVSR approach zero, therefore an equilibrium must be take. For the analysis in this dissertation, three seconds will be considered starting from the short-circuit application instant.

2.6 Grid-Tied Converters' Impacts on Short-Term Voltage Stability and Existing Research

Reference [7] presents an analytical method to asses short-term voltage stability (STVS) using dynamic PV-plane (active power versus bus voltage) for induction motor load. The short-term voltage instability is not related to the "nose" as usually presented in works for long-term voltage stability, thus, the boundary for instability depends on the remaining torque (the difference between electrical and mechanical torque) in the induction motor, if it is positive after the disturbance, the motor can accelerate and the system can recover stability. Therefore, this paper presents a methodology to draw the boundary stability in the PV plane and assess the STVS

properly.

The works [15, 26, 27] use the transient PV curve to asses STVS according to the methodology described in [7]. The paper [15] presents an analysis of how the FRT function affects STVS. The article [26] discusses reactive current prioritizing in case of short-circuit and the effects on the system instability and then, proposes a methodology that allows both active and reactive power to be injected into the system during a fault. Reference [27] presents a methodology to asses short-term voltage stability in the case of a parallel operation of an inverter and a synchronous generator.

Reference [28] presents an analysis of Multi-Infeed of voltage source converter (VSC). The Multi-infeed scenario is characterized by the electrical proximity of equipment connected to the network, this kind of operation in weak networks might experience some problems like adverse interference among each other. The paper [28] shows that the voltage damping presents a low value when two or more VSCs are connected to the grid when their controller design does not consider the presence of other VSC. Hence, this paper presents a tuning methodology to avoid this issue.

A controller based on state feedback is presented in reference [29] to improve the short-term voltage stability margin. This paper also addresses the effect of wind turbines based on fixed-speed induction motors on instability, its behavior is similar to induction motor load but instead of deceleration, the wind turbine accelerates.

HOSSAIN *et al.* [30] proposes an analysis methodology based on a linear model that includes not only the linear term in the Taylor series but also the Cauchy remainder. The Cauchy remainder is an uncertain term that makes the linear model better representative, once it represents the model with more accuracy around the equilibrium point. The book [31] uses this methodology to improve power electronics device control in general.

For this dissertation, the power system benchmark used for the analysis is taken from reference [7] with some changes: two lines were added between buses 2 and 3, besides the parameters were changed as presented in Section 4.1. Although the mathematical model proposed in [7] is useful for this type of analysis, in this document it was not chosen, instead simulation analysis was performed. The vectorial controllers will be embedded with the method proposed in reference [26] for the comparative analysis.

Chapter 3

Theoretical Foundations

3.1 Mathematical Background

This section aims to provide insight into the mathematical aspects of nonlinear system dynamics and its stability, which are essential to understanding the qualitative behavior of voltage stability such as the existence of unstable equilibria, and bifurcations.

3.1.1 Ordinary Differential Equation

Power system dynamics can be represented by the compact equation:

$$\frac{d\mathbf{x}}{dt} = \mathbf{f(x)}, \tag{3.1}$$

where $\mathbf{x}$ represents an $n \times 1$ state vector composed of n x_i components and, $\mathbf{f}$ represents a vector composed usually by a nonlinear function in the form of $f_i(\mathbf{x})$. The x_i component represents physical quantities of the power system, such as voltage, current, or control variables, as well as, it might be a mathematical variable. The function $f_i(\mathbf{x})$ is derived from physical laws such as Kirchhoff's laws, Newton's laws, and, control strategies.

The time response of a nonlinear system is obtained by solving the nonlinear Equation (3.1) from an initial condition known at a certain time instant:

$$\mathbf{x}(t_0) = \mathbf{x}_0 \tag{3.2}$$

The vector $\mathbf{x}$(t) for $t > t_0$ for any $\mathbf{x}_0$ pictures a trajectory in the state space. The stability of this solution is essential to ensure the reliable and safe operation of the power system.

Nonlinear systems are complex and challenging to solve analytically. However, numerical methods can effectively solve them. In this master's dissertation, the

systems are analyzed numerically using PSCAD™/EMTDC™ [32].

3.1.2 Stability Definition and Equilibrium

The equilibrium points of the system defined in Equation (3.1) are any $\mathbf{x}^*$ point that solves the equation:

$$\mathbf{f}(\mathbf{x}) = \mathbf{0}, \tag{3.3}$$

if $\mathbf{x}_0 = \mathbf{x}^*$ and there is no disturbance in the system, the solution for all time is $\mathbf{x}(t) = \mathbf{x}^*$, once all the derivatives are zero, the system does not "move" along any trajectory.

An equilibrium point is classified according to its stability (the stability definition adopted in this dissertation is related to Liapunov [33]):

- $\mathbf{x}^*$ is said to be stable if for any initial condition $\mathbf{x}_0$ in the neighborhood of $\mathbf{x}^*$, the trajectory $\mathbf{x}$(t) remains close to $\mathbf{x}^*$ for all time;
  - $\mathbf{x}^*$ is said to be asymptotically stable if all trajectories starting from $\mathbf{x}_0$ in the neighborhood of $\mathbf{x}^*$ approaches $\mathbf{x}^*$ as $t \to \infty$;
- $\mathbf{x}^*$ is said to be unstable if does not meet the above criteria.

Region of Attraction

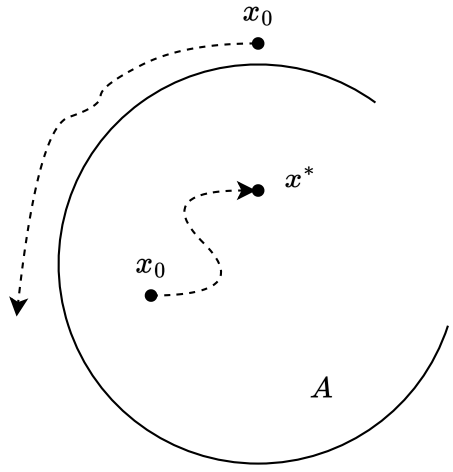

Figure 3.1: Region of attraction for a two-dimensional system.

The definition of stability is a local property of the system since it is related to an equilibrium point. A global behavior for the system is the region of attraction also known as the basin of attraction or domain. The basin of attraction is defined as the largest set A in the state space in which every $\mathbf{x}_0 \in A$ leads the trajectory to approach $\mathbf{x}^* \in A$ asymptotically, Figure 3.1 shows a two-dimensional example.

3.1.3 Phase Portrait

The phase portrait of a system is a diagram containing its equilibrium points and arrows indicating the flow of the state vector $\mathbf{x}$. For the system:

$$\frac{dx}{dt} = \mu - x^2, \tag{3.4}$$

three phase portraits are shown in Figure 3.2, depending on the value of μ.

It is possible to see if the arrows approach the equilibrium point, it is a stable point, and if the arrows move away from the equilibrium point it is an unstable equilibrium point. In the third case, as $\mu < 0$, there is no equilibrium point, considering that $\frac{dx}{dt} < 0 \ \forall \ t > t_0$, the diagram is only an arrow pointing to the left.

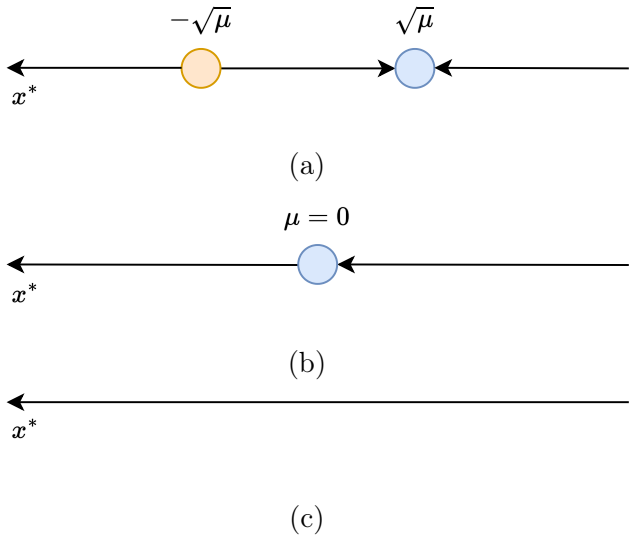

Figure 3.2: Phase portrait for the Equation (3.4)
(a) $\mu > 0$, (b) $\mu = 0$ and (c) $\mu < 0$.

3.1.4 Bifurcations

Bifurcation of a non-linear system means a qualitative change in the phase portrait topology by varying one or more parameters of this system [34]. In this section, only the saddle-node bifurcation will be explained. Although the Hopf bifurcation is also important for voltage stability understanding, this will not be addressed in this dissertation which focuses on voltage collapse.

Saddle-Node Bifurcation

Saddle-node bifurcation is a condition of some non-linear systems where the variation of one or more parameters creates or destroys a pair of equilibrium points with opposite stability [34].

An example is the Equation (3.4), that presents two equilibrium points $x^*_{1,2} = \pm\sqrt{\mu}$ if $\mu > 0$.

Figure 3.3 shows the bifurcation diagram for the Equation (3.4). The phase portrait assumes a different form for $\mu < 0$ when compared to $\mu > 0$.

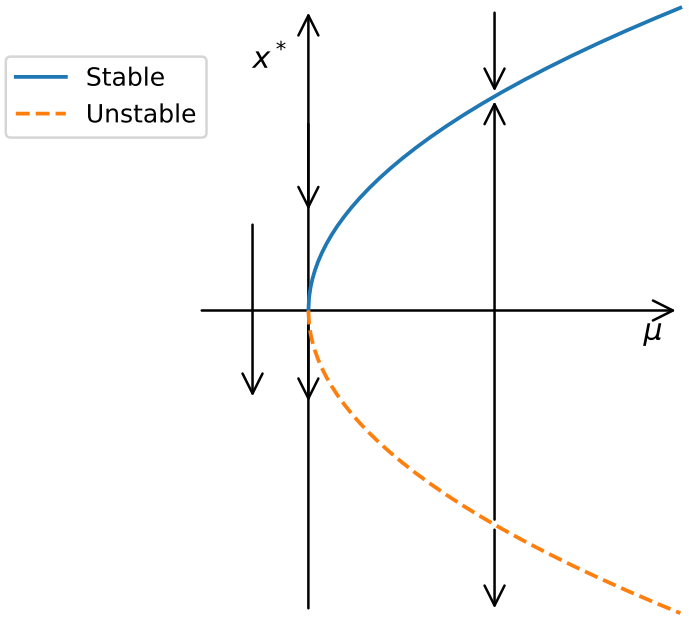

Figure 3.3: Bifurcation diagram for $\frac{dx}{dt} = \mu - x^2$.

This system presents one eigenvalue for each equilibrium point if $\mu > 0$. For $x^*_1 = \sqrt{\mu}$, the eigenvalue is $\lambda = -2\sqrt{\mu}$, so, it is an asymptotically stable equilibrium point. For $x^*_2 = -\sqrt{\mu}$, the eigenvalue is $\lambda = 2\sqrt{\mu}$, so, it is an unstable equilibrium point.

If $\mu = 0$, the eigenvalue becomes zero, and for $\mu < 0$ there is no equilibrium point.

Therefore, $\mu = 0$ is the bifurcation point where the saddle-node bifurcation happens. Above zero, there are two equilibrium points with opposite stability, and below zero, there are no equilibrium points.

3.2 Voltage Stability and Instability Definition

A power system that is capable of maintaining its voltage to acceptable levels after a large or small disturbance, is referred to as a stable system regarding voltage stability. This ability depends on the whole network to be able to transfer the required energy to the load center [1].

An alternative definition, however for instability is provided by [33]. This definition says that voltage instability concerns the load recovery characteristic in restoring itself beyond the system capacity. This definition is illustrated in the flowchart

in Figure 3.4.

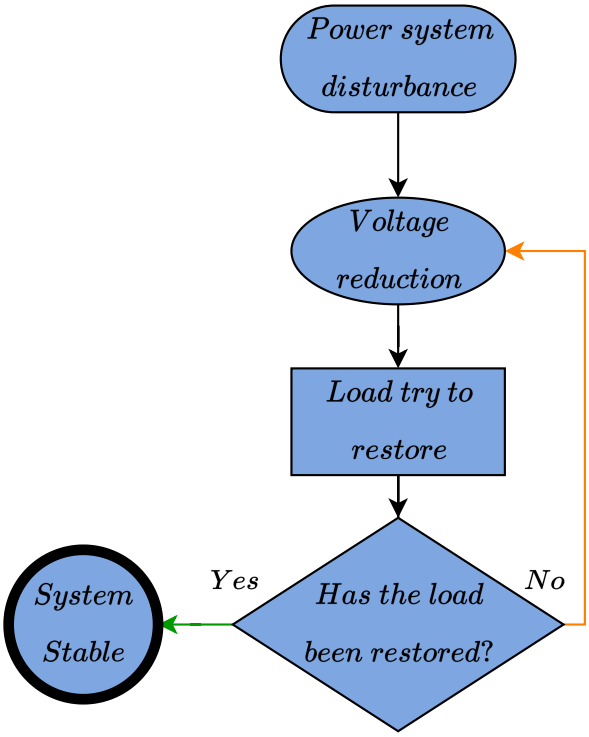

Figure 3.4: Voltage instability load driven flowchart.

The voltage stability is divided according to the time of action, these are: short-term voltage stability (STVS) and long-term voltage stability (LTVS) [33].

3.3 Short-Term Voltage Related Instability

Short-term voltage-related instability is a fast phenomenon in the order of zero to ten seconds. It is closely related to fast-acting devices in the power system. According to [5], there are four types of short-term voltage-related instability issues:

- Short-term voltage Instability (STVI);
- Transient Rotor Angle Instability (TRAI);
- Fault-induced Delayed Voltage Recovery (FIDVR);
- Converter-Driven Slow Interaction Instability (CSII).

3.3.1 Short-Term Voltage Instability (STVI)

The STVI is the best-known type of short-term voltage-related instability phenomena [5] and it is mainly related to the load's dynamic and is the focus of this work.

Short-term voltage instability is defined as a fast deterioration of the voltage due to the dynamic of fast-acting devices (eg.: HVDC, Induction motors, and others) [33]. Otherwise, it is possible to understand voltage instability as the inability of the power system to deliver the requested power to the loads.

The most common cause of voltage instability is normally associated with the HVDC link and induction motor. Both need a large amount of reactive power to work properly which interacts adversely with the voltage in power systems with large reactance [35]. This is especially bad in case of short-circuit or other disturbance near the load center which deteriorates the voltage and because of the load dynamic behavior, the voltage might be unable to recover, leading to the voltage collapse [36].

However, the recent interest in renewable energy has increased the connection of IBG to the grid, once dominated by synchronous machines, turning the voltage stability issue into a phenomenon much more complex [5].

The STVI has three basic mechanisms, these will be explained in Section 3.7:

- Loss of a short-term dynamic equilibrium point after a disturbance (STM1);
- Lack of attraction of the short-term dynamics to the region of attraction (STM2);
- Oscillatory instability (STM3).

3.3.2 Transient Rotor Angle Instability (TRAI)

Transient rotor angle instability is a widely known phenomenon of stability. Its definition is related to the rotor angle which after a disturbance is unable to remain synchronized with the system.

The loss of synchronism can happen by undamped electromechanical oscillations or in the form of a monotonic rotor acceleration/deceleration [37].

The rotor angle instability is a phenomenon that normally does not happen alone and it is difficult to identify clearly the difference between this and short-term voltage instability. Figure 3.5 shows two cases where both phenomena happen separately.

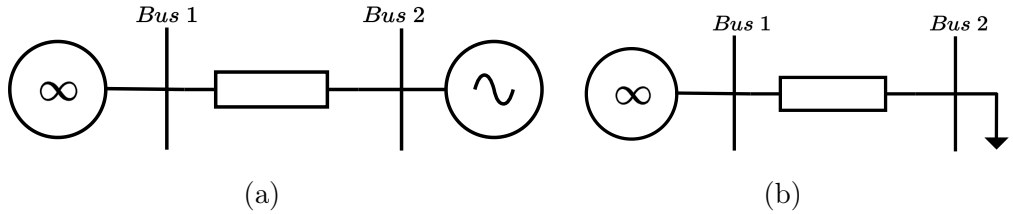

(a) (b)

Figure 3.5: Case where there is only (a) angle instability and (b) voltage instability.

The system shown in Figure 3.6 is prone to both STVI and TRAI, but in this case, only STVI will happen. The parameters of the system are described in Chapter 4. The voltage after a short circuit is shown in Figure 3.7a which was unable to recover itself, but the machine close to the load remained synchronized as shown in Figure 3.7b.

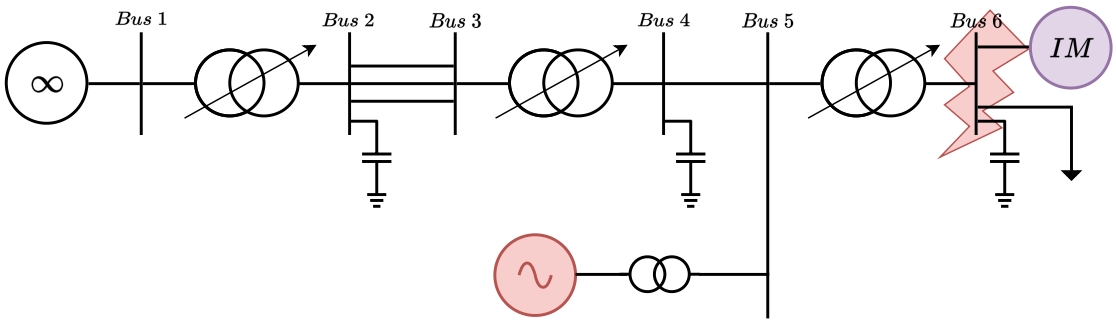

Figure 3.6: Case where there is a dynamic load and a synchronous machine far from the big system and only voltage instability is present.

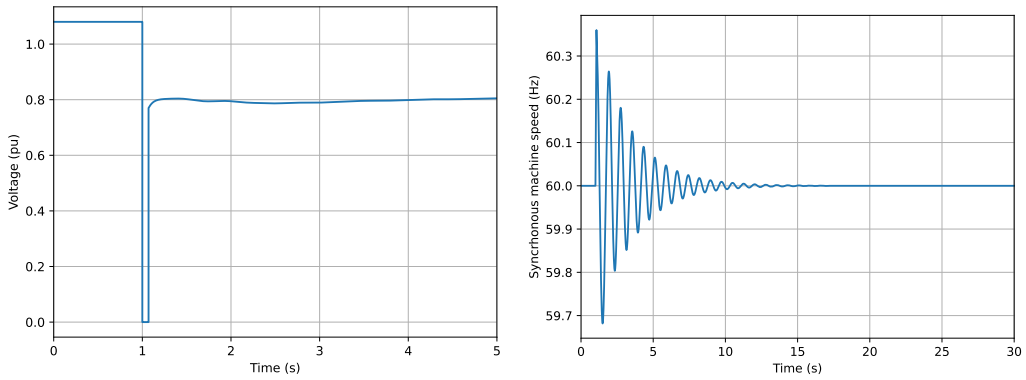

(a) (b)

Figure 3.7: Case where there is only voltage instability (a) voltage and (b) synchronous machine speed.

3.3.3 Fault-Induced Delayed Voltage Recovery (FIDVR)

Fault-induced delayed voltage recovery represents a novel phenomenon in terms of research and industry interest. This phenomenon can be defined as a too-slow recovery of the voltage after a disturbance [5, 36].

The small induction motors connected to the grid, usually single-phase induction motors in the distribution system, are susceptible to stalling because of their low inertia. The stalling of a large number of them causes the phenomenon called Fault-induced Delayed Voltage Recovery.

The small motors connected to the distribution system commonly trip from the grid through thermal protection while the big ones trip through under voltage

protection. When there is a stall of an induction motor there is a large consumption of reactive current leading to a depression of the voltage and the delayed recovery of the system.

Some FIDVR events have occurred as presented in [36]. The majority of them occurred in residential load areas in periods of high temperature led by stalling of air conditioners induction motors. Reference [38] states that this phenomenon occurred in the BIPS in 2019 in the southeastern region after a short circuit.

3.3.4 Converter-Driven Slow Interaction Instability (CSII)

The Converter-Driven Slow Interaction Instability was recently added to the stability definition by the IEEE Task Force [1], to contemplate the arising of inverter-based generation across the world.

CSII is the instability driven by the interaction of slow dynamics of the converter's control and the power system. This phenomenon affects both voltage and frequency stability. In [36] this phenomenon is classified as closely related to voltage stability.

3.4 Long-Term Voltage Instability (LTVI)

Long-term voltage instability (LTVI) is the most well-known type of voltage instability [5]. It is characterized by a modification in the voltage of buses driven by slow equipment action (eg.: OLTC, thermostatically controlled load, slow increase of load, etc).

The study period of analysis may vary from some seconds to several minutes [9], so long-term simulation analysis is necessary.

This type of instability normally happens due to the loss of long-term dynamics equilibrium point, caused by load dynamics trying to restore its active power consumption beyond the capacity of the network [1].

If the short-term dynamics are stable after a disturbance, the system is governed by the long-term dynamics or slower state variables. As a result, if the system is governed only by the long-term variables three basic mechanisms might lead to LTVI [33]:

- Loss of a long-term dynamics equilibrium point after a disturbance (LMT1):
  - After a disturbance the equilibrium point disappears as in a saddle-node bifurcation;
  - An example is removing a transmission line in a system with an On Load Tap Changer (OLTC). After the short-term dynamics die out, the OLTC

starts trying to recover the load, but if it is unable to do so because there is no equilibrium point, then the system voltage collapses.

- Loss of attraction of the long-term dynamics to the region of attraction (LTM2):
  - After the disturbance, the state vector goes beyond the region of attraction limit which makes it impossible to reach the equilibrium point;
  - An example is, after the example given for the LTM1 mechanism, the operator takes longer in the corrective action like a load shedding for instance. This action can recover the equilibrium point, but if the operator takes longer to act the state vector goes beyond the attraction region, therefore the system is not able to reach the equilibrium point.
- Slow-growing voltage oscillation (LTM3):
  - According to [33] this instability mechanism was not observed in real power systems and it is related to oscillatory instability.

It is worth mentioning that the system might also achieve short-term instability by the change of the slow variables, which act as a parameter for the short-term dynamics. There are also three mechanisms of this instability:

- Loss of short-term equilibrium caused by long-term dynamics (S-LTM1):
  - A case where this instability might appear is when the degradation caused by long-term variables like the tap of an OLTC causes a loss of synchronism in the system;
  - In this case the long-term variables act as a parameter to the short-term variables, so its variation might lead the system to a saddle-node bifurcation point or even to a Hopf bifurcation.
- Loss of attraction to the stable short-term equilibrium due to shrinking region of attraction caused by long-term dynamics (S-LTM2):
  - This instability might appear after the reduction of the basin of attraction caused by the long-term variables' action. Even a small disturbance can move the state vector outside the region of attraction.
- Oscillatory instability of short-term dynamics caused by long-term dynamics (S-LTM3):
  - This instability mechanism could happen in a system that presents both voltage and electromechanical oscillation problems and it is related to Hopf bifurcation also.

3.5 Load Aspects Regarding Voltage Stability

The load is one of the main factors of STVI [33]. Its dynamic plays a key role in the power system voltage instability, so load comprehension and accurate modeling are crucial for voltage instability assessment.

In real power systems, load modeling is challenging. The real load is aggregated, and the effect seen from a substation is the combination of all loads. In the literature, it is possible to find a lot of works trying to represent the aggregate aspect [18].

This section intends to present the common loads and their differences in the voltage stability assessment.

3.5.1 Load Definitions

The general model of the load is given by:

$$P = P(x, V, t) \tag{3.5}$$

$$Q = Q(x, V, t), \tag{3.6}$$

where P and Q are respectively the active and reactive powers. x is a state variable, V is the voltage and t is the time.

Static Load

The well-known static load is represented by:

$$P = zP_0 \left(\frac{V}{V_0}\right)^{\alpha}, \tag{3.7}$$

$$Q = zQ_0 \left(\frac{V}{V_0}\right)^{\beta}. \tag{3.8}$$

the subscript 0 indicates a reference value. z is the load demand. α and β are used to model different types of load. This load representation does not present a dynamic dependence nor time and state variables are present, but its value might vary with time caused by a voltage variation.

Dynamic Load

There are different types of dynamic loads, their main characteristic is that they tend to restore their power consumption whether by the control system or their own dynamics after a voltage reduction.

The loads normally used for voltage stability assessment are induction motor, static load connected to an OLTC, or thermostatic load [33]. The induction motor is a fast action load, and it is normally related to short-term voltage stability while the static load connected to OLTC and the thermostatic load are of slow action type and they are related to long-term voltage stability.

Static Load Versus Dynamic Load

Figure 3.8 shows the difference in short-term voltage stability for both static and dynamic loads. The dynamic load is an induction motor, and its model is described in Chapter 4.

In [39], different compositions of loads are studied, but only the lack of attraction to the equilibrium point mechanism is studied. Figure 3.8a shows the difference in time response to a short circuit for the same time duration, as can be seen, the static load is capable of regaining stability, while the dynamic load is not.

In this dissertation, the difference in load composition for the saddle-node instability mechanism is also addressed, Figure 3.8b shows the response to the reactance variation, as can be seen, the dynamic loads reach the bifurcation point first.

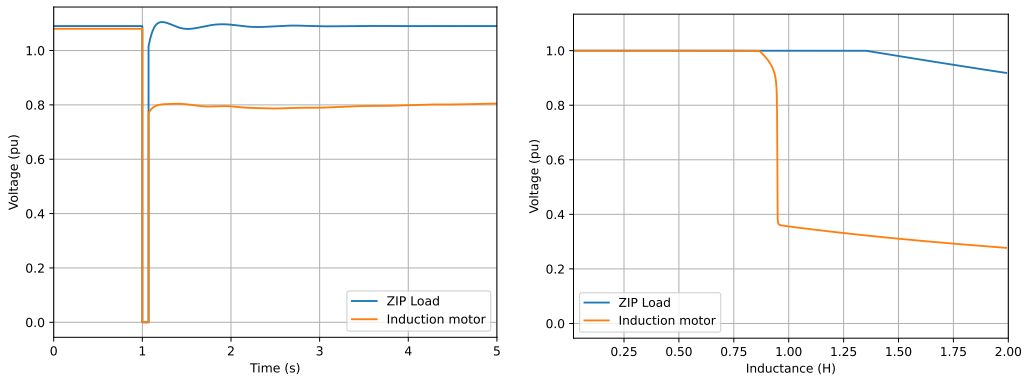

(a) (b)

Figure 3.8: Difference for the static and dynamic load (a) loss of equilibrium of short-term dynamics and (b) loss of equilibrium point.

3.6 Power System's Power Plants

The power plants of the power system must be modeled properly for voltage stability assessment. Their dynamic affects directly the voltage stability whether short-term or long-term. Synchronous machines are the main source type in the EPS, their voltage control, and their limits influence the system behavior and must be modeled.

As the IBG presence in the EPS has been increased and their controllers also affect the voltage stability of the system, they must be studied and appropriately

modeled. The HVDC system might act as a source in part of the system. If the HVDC is of a line-commutated converter (LCC) type, it always needs reactive power whether as a rectifier or inverter, which is a problem for the voltage control and stability.

3.7 Short-Term Voltage Instability Mechanisms

As already pointed out in Section 3.3.1, a short-term voltage instability might arise in the power system by three mechanisms [33]. STM1 and STM2 will be explained in detail in this section while STM3 will not be explained, because it will not be addressed in this dissertation which focuses on voltage collapse. The system shown in Figure 3.9 will be used to demonstrate the mechanisms.

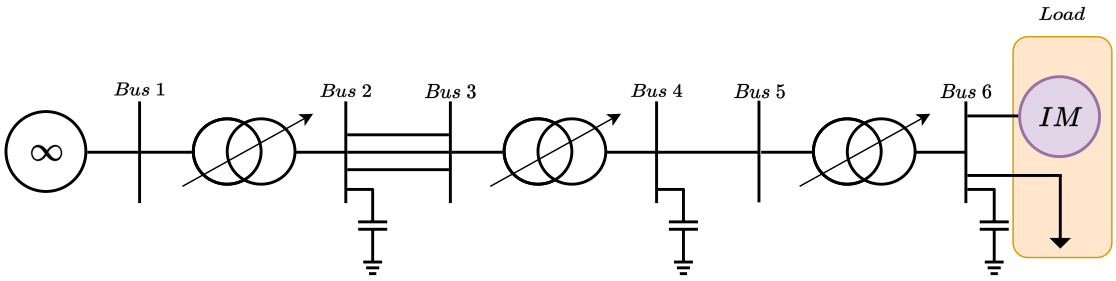

Figure 3.9: Power system used for the analysis.

3.7.1 STM1: Loss of Equilibrium Point

The STM1 mechanism is a loss of equilibrium point through variation of one parameter of the system.

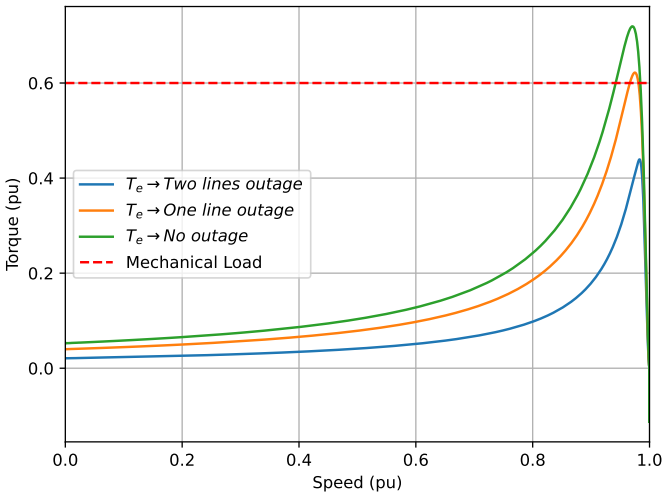

Figure 3.10: Static characteristic of an induction motor torque for different conditions of line outage.

An example of this mechanism can be seen in Figure 3.10, where three static curves for the induction motor for each state of the network, characterized by line outages, can be observed. The electromagnetic torque (T_e) is plotted as a function of the mechanical speed. For no or one-line outages there are equilibrium points, but for the two-line outage, the equilibrium point disappears as there is no intersection between the mechanical load, modeled as a constant torque, and the electromagnetic torque. Figure 3.11 shows the time response for one and two-line outages.

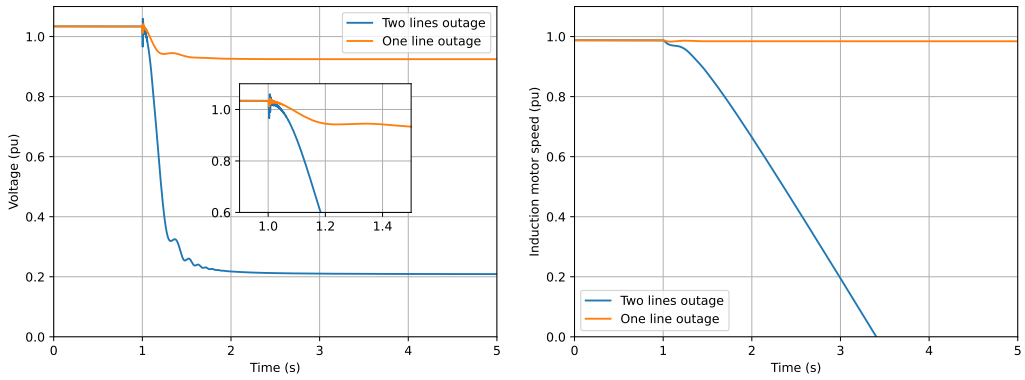

(a) (b)

Figure 3.11: Dynamic response for line outages (a) voltage and (b) induction motor speed.

3.7.2 STM2: Lack of Attraction to the Equilibrium Point

The STM2 mechanism is a lack of attraction to the equilibrium point after a disturbance. An example of this mechanism is a short circuit with a different time duration. Figure 3.12 shows the time response for two short circuits. It is possible to see that for 60 ms of short circuit, the system can recover stability, but it is unable for 70 ms of short circuit.

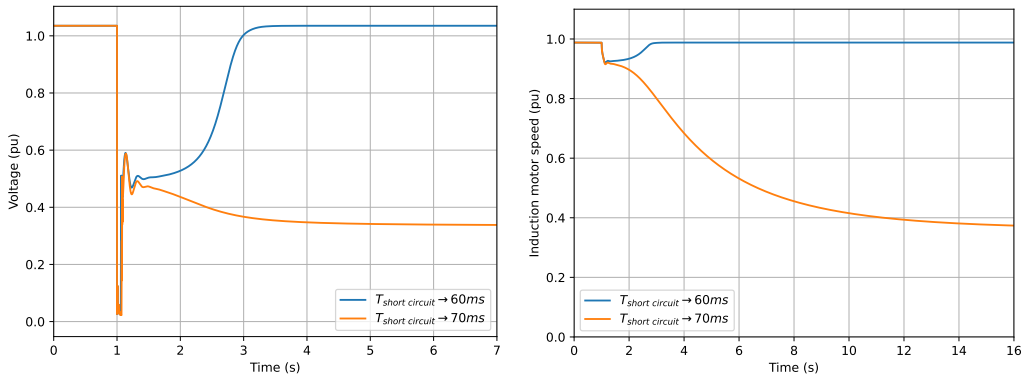

(a) (b)

Figure 3.12: Dynamic response for two short circuit durations (a) voltage and (b) induction motor speed.

3.8 Countermeasures for Short-Term Voltage Instability

To avoid short-term voltage instability issues, there are a lot of countermeasures that can be taken. Some of them are [33]:

- Fast capacitor switching:

  Capacitors connected through switches can be quickly connected to the system.

- Static Var Compensators (SVC):

  SVCs are fast-acting devices that can control the system voltage and enhance the system stability.

- HVDC modulation:

  HVDC system based on thyristors needs reactive power to operate. As the HVDC control is fast, it can reduce the reactive power demand, lowering its active power.

- Fast fault clearing:

  As explained in Section 3.7.2, the fault time duration plays an important role in short-term voltage instability. Consequently, fast fault clearing can keep the system stable.

- Load shedding:

  When the system starts going into a voltage instability mechanism, the load shedding can avoid instability.

- Upgrade the system or add more transmission lines:

  This action is currently taken in a power system because the demand increase is a constant process, that being the case, it is necessary to enhance the power system to guarantee reliability and safe operation. However, it is a planning solution that takes some years to start operating.

3.9 Improvements in the Dynamic Voltage Support to Improve Stability Margin

KAWABE *et al.* [26] proposed a methodology to improve short-term voltage stability in a system that contains a power converter with control in *dq*-Frame. It is based

on changing the dynamic voltage support (DVS), which will be explained further in Section 4.2.2 and will be adapted to the control in $\alpha\beta$-Frame in Section 4.2.3. The system shown in Figure 3.13 will be used to show the proposal, the parameters for the simulation, and the structure of the controllers will be presented in Chapter 4.

The DVS proposed in the article is based on changing from reactive current prioritizing during a disturbance as recommended by ONS instruction, presented in Section 2.4.1 to injecting active power also, during the disturbance.

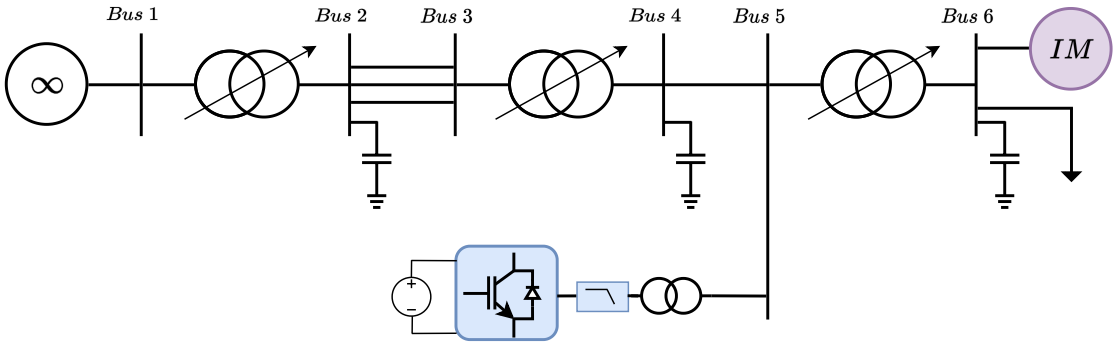

Figure 3.13: Power system structure used to show the improvements on the IBG's control.

Figure 3.14 shows the voltage response to a short circuit for both the conventional DVS and the proposed in reference [26]. As can be seen, the control strategy proposed in [26], called smart DVS, recovers the voltage faster than the conventional one.

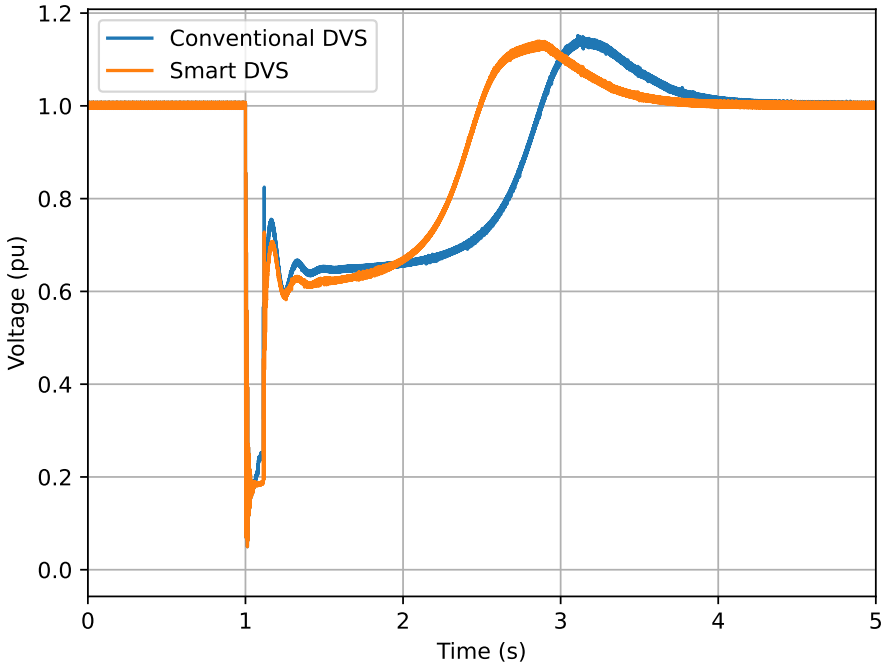

Figure 3.14: Voltage recovery for different DVS.

Figure 3.15 shows the output of the converter for both DVS. In the conventional, the active power goes to zero during the disturbance while in the smart one, the active power achieves almost the same value as the reactive power during the disturbance. The current magnitude is shown for both cases to be almost 1 *pu* during the disturbance. As regular power converters have their thermal limits, it is necessary to guarantee a controlled current magnitude during the disturbance to avoid damaging the converter's switch.

A large disturbance like a short circuit can also lead the system to short-term frequency instability. As the smart DVS injects active power during the disturbance it helps the system reduce the frequency deviation.

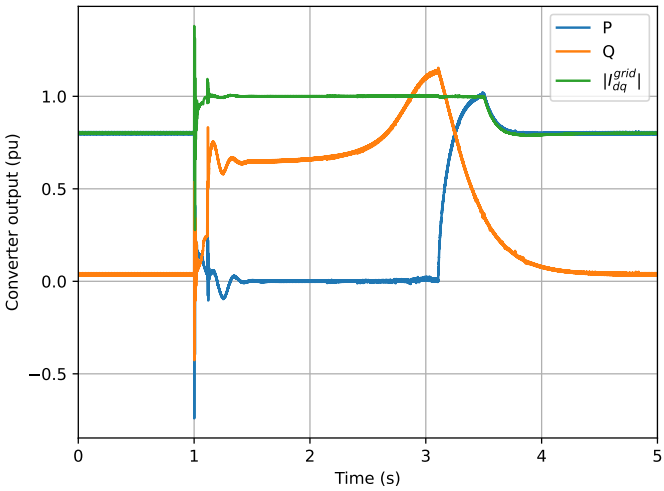

(a)

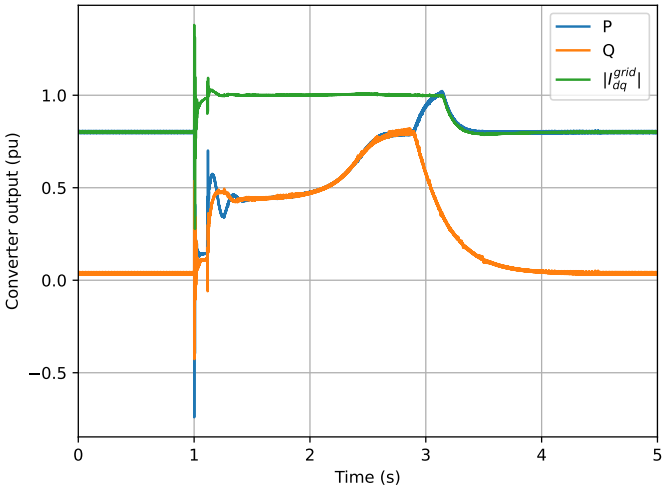

(b)

Figure 3.15: Converter output for different DVS (a) conventional and (b) smart.

Table 3.1 shows the Critical clearance time (CCT) of a short circuit for both DVS. The smart DVS presents better resilience to the short circuit, it is able to support a longer short circuit time duration, 122.8 *ms* before instability, while the

conventional one is not.

.

Table 3.1: CCT for different DVS.

DVS type	**CCT (ms)**
Smart	122.8
Conventional	117.6

Regarding the saddle-node stability margin, Figure 3.16 shows the response for reactance increase for both DVS. As can be seen, the smart one shows a better result as it needs a longer reactance to start the voltage collapse.

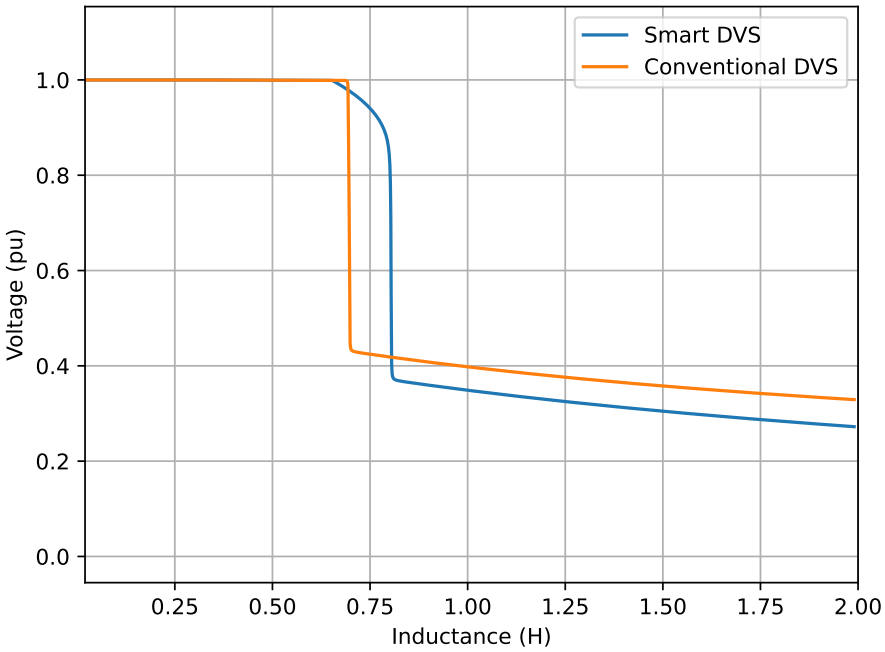

Figure 3.16: Saddle-node stability analysis for different DVS.

Chapter 4

Case Study Structure

4.1 Test System Structure

The system used in the case study is shown in Figure 4.1. It was adapted from [7] and is known to be susceptible to short-term voltage instability due to its high impedance between the strong network (represented as an infinite bus) and the load center. The system includes a source located close to the load, but its capacity (50 MVA) is smaller than that of the load (250 MW, 86 MVAr), composed of an induction motor (150 MW, 86 MVAr) and a constant impedance static load (100 MW, 0 MVAr). The switch S_1 and S_2 are used to connect the local source to the system, however, both are never on at the same time, the local source is an inverter or a synchronous machine.

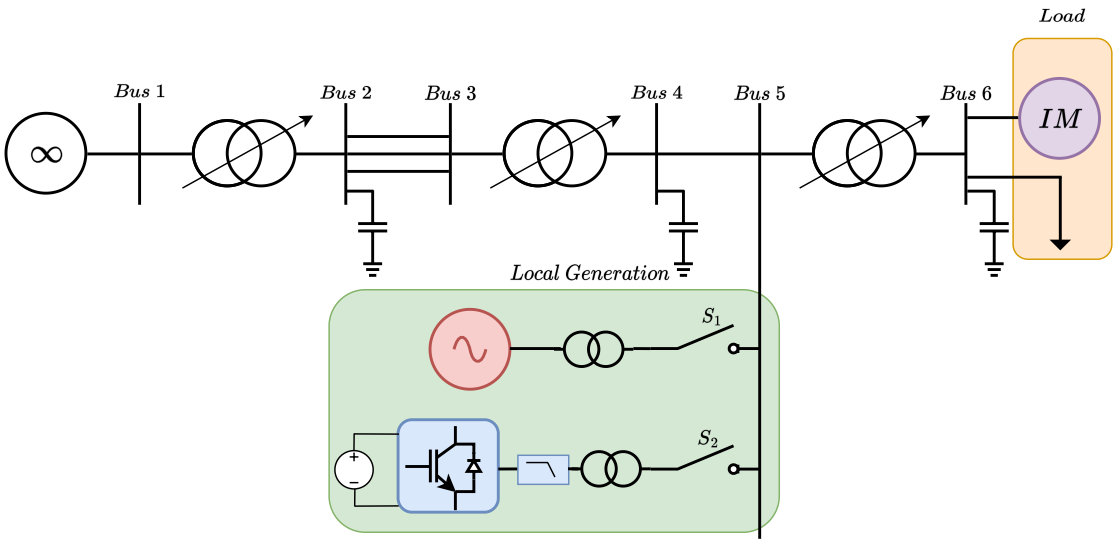

Figure 4.1: Power system used for the analysis.

Figure 4.2 depicts the operation point of the system for all the analysis. The capacitors' susceptance and the static load conductance power are shown for nominal

voltage (1 pu).

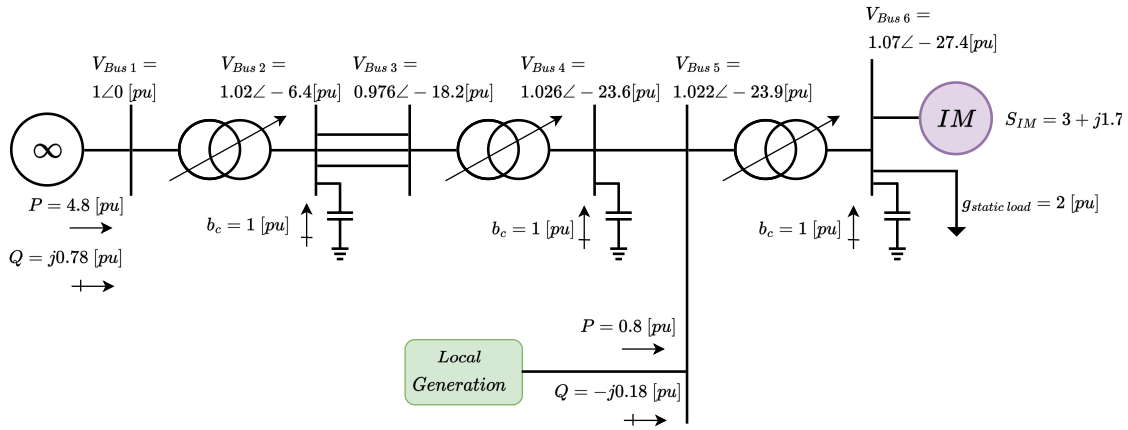

Figure 4.2: Power flow of the power system used in the analysis.

The system's parameters are shown in Tables 4.1, 4.2, and, 4.3, respectively induction motor, transformers, and, transmission lines parameters.

Table 4.1: Induction motor parameters.

Parameter	**Value**
S_{im}	250 MVA
V_{ll}	13.8 KV
ω_0	$2\pi 60$ rad/s
J	1.2 s
R_s	0.02 pu
R_r	0.02 pu
L_m	4 pu
L_s	0.1 pu
L_r	0.1 pu

Table 4.2: Transformers parameters.

Bus from	**Bus to**	**X(pu)**	**Rated MVA**	**Connection**
1	2	0.02	50	YY
3	4	0.015	50	YY
5	6	0.012	50	YY
Converter	5	0.1	50	ΔY

Table 4.3: Transmission line parameters.

Bus from	**Bus to**	**R(pu)**	**X(pu)**	**Rated MVA**	**Circuit number**
2	3	0.006	0.11	50	1, 2 and 3
4	5	0.0005	0.002	50	1

4.2 Power Converter

This section presents the power converter used for the analysis. Section 4.2.1 presents the converter and its connection to the system. Sections 4.2.2, 4.2.3, and 4.2.4 present respectively control in dq-Frame, control in $\alpha\beta$-Frame and synchronverter control, which are all the control philosophies used in this research study.

4.2.1 Converter Structure

The power converter utilized is a two-level voltage source converter [40] with an Inductor-Capacitor-Inductor filter (LCL), which was designed following the methodology described in [41]. Figure 4.3 shows the schematic of the converter and its connection to the system.

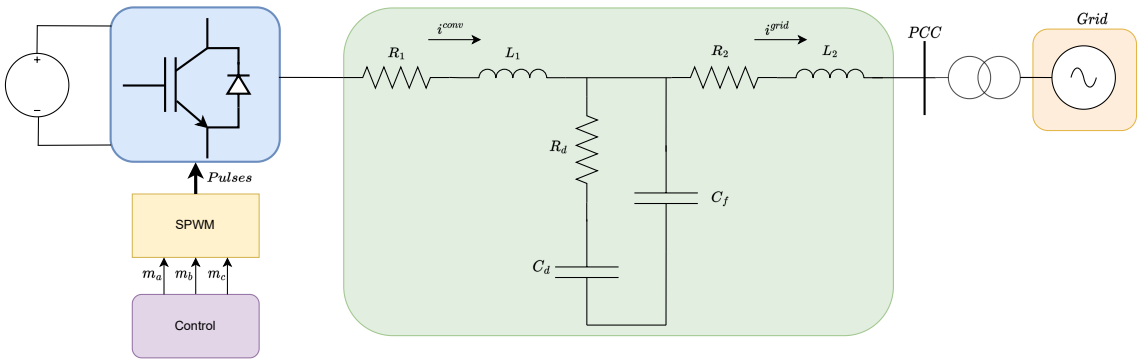

Figure 4.3: Converter structure.

To enable a generic analysis, the DC side was represented by an ideal DC voltage source. In an actual system, it can be a solar panel or a synchronous generator linked to wind turbines, among others.

The sinusoidal pulse width modulation method [40] is employed to generate the pulses to the transistors, and the reference signals for the modulation, m_a, m_b, and m_c, are determined by the control law employed.

The parameters of the converter are shown in Table 4.4. These values are not commonly used for a two-level voltage source converter, however, it is employed as representing an equivalent power converter. Therefore, a two-level voltage source converter will be used for the analysis.

Table 4.4: Power converter parameters.

Parameter	Value
V_{ll}	113 kV
S_N	50 MVA

The LCL parameters calculated are presented in Table 4.5.

Table 4.5: LCL filter parameters.

Parameter	Values	
	Real	**Pu**
R_1	1.65 Ω	6.46×10^{-3}
L_1	88 mH	1.29×10^{-1}
R_d	490 Ω	1.918
C_d	0.8 μF	7.702×10^{-2}
C_f	0.8 μF	7.702×10^{-2}
R_2	1.13 Ω	4.42×10^{-3}
L_2	60 mH	8.86×10^{-2}

4.2.2 Control in *dq*-Frame

The control in the *dq* reference frame used for the analysis is described in this section. This control is a cascaded control based on two loops, the internal one which is a current loop, and the outer one which in the literature assumes different forms [40].

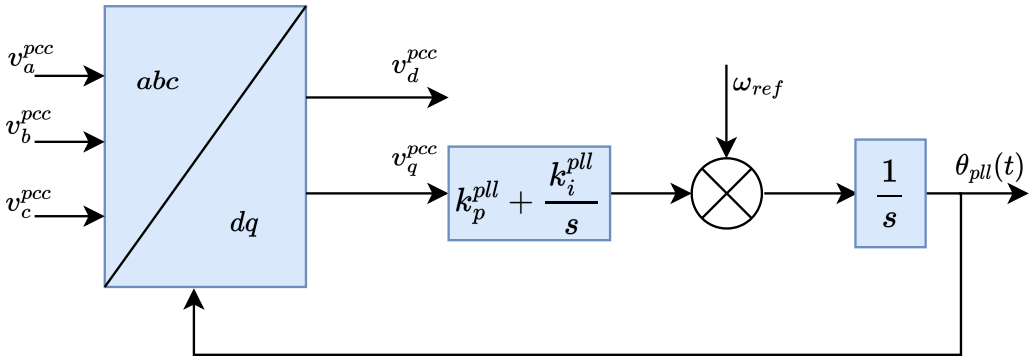

Figure 4.4: SRF-PLL.

This control philosophy needs the park's transform [40], to do so it is necessary to detect the instantaneous phase angle of the voltage at the PCC. In this research, it is used a Synchronous reference frame - Phase-locked loop (SRF-PLL) [42] as shown in Figure 4.4 to detect the phase angle, the parameters used for the SRF-PLL are shown in Table 4.6.

Table 4.6: SRF-PLL parameters.

Parameter	Value
k_p^{pll}	50
k_i^{pll}	900

Figure 4.5 shows the internal loop based on a Proportional Integral (PI) control. This control system topology aims to generate a modulation index reference which makes the current flowing through the L_2 inductor follow the reference given by the outer loop. In the *dq* reference frame, the desired steady-state values are constant,

making it possible to use a PI control. This loop also presents a decoupling term that makes the currents, independent from each other during a transient in an ideal scenario, the PI parameters designed according to the methodology in the Appendix A are shown in Table 4.7.

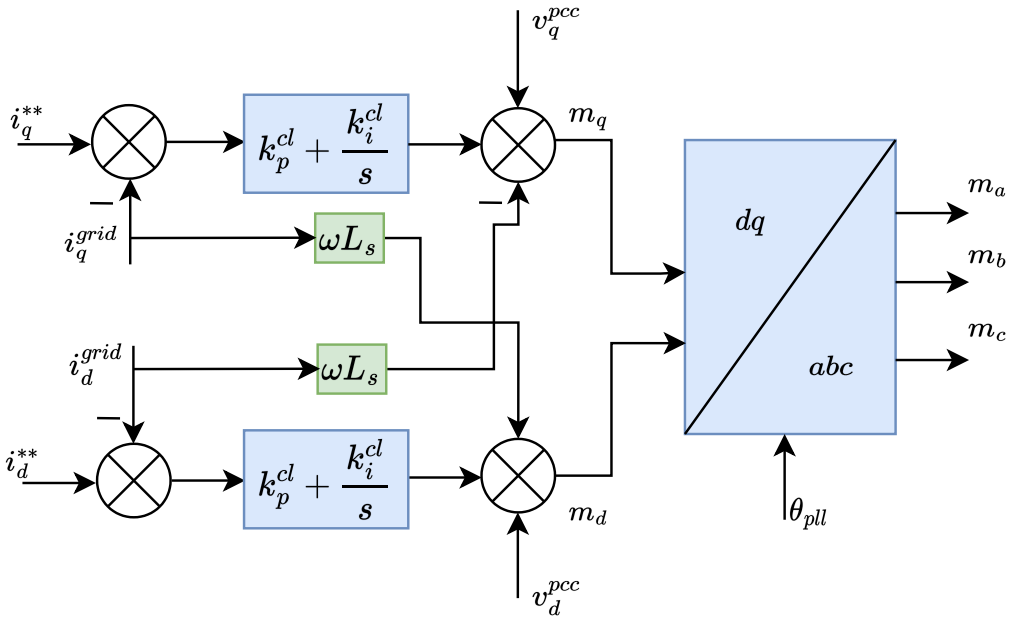

Figure 4.5: Inner loop control in *dq*-Frame.

Table 4.7: Current loop parameters for the control in *dq*-Frame.

Parameter	**Value**
k_p^{cl}	0.1449
k_i^{cl}	2.7214

The outer loop is responsible for generating the reference currents. If the SRF-PLL angle synchronizes into one axis, the active and reactive power gets decoupled in terms of the q and d-axis currents. This way the reactive current can be generated by a PI that compares the terminal voltage and the same happens to the active current, but it comes from an active power comparison as shown in Figure 4.6, the parameters used for the comparative analysis are shown in Table 4.8.

Table 4.8: Outer loop parameters for the control in *dq*-Frame.

Parameter	**Value**
k_p^{apl-dq}	0.04
k_i^{apl-dq}	10
k_i^{vl-dq}	0.06102
k_i^{vl-dq}	15.2571

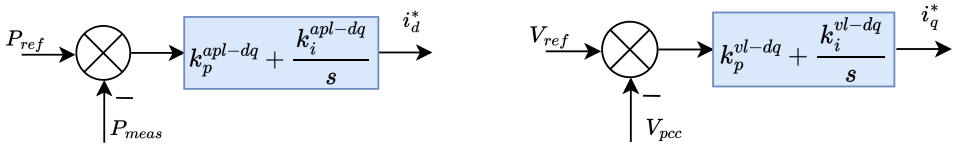

(a) (b)

Figure 4.6: Control in dq-Frame outer loop (a) active power outer loop and (b) voltage outer loop.

After the outer loops have generated the reference currents it is necessary to pass them through a limiter, which will adjust the current's magnitude according to the converter capacity. This dissertation adopted the method proposed in [26].

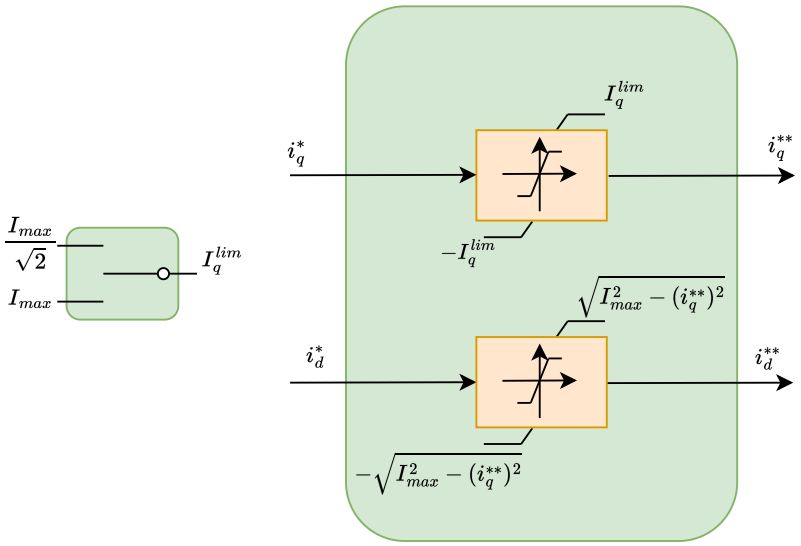

Figure 4.7: Current limiter.

Figure 4.7 shows two ways of limiting the direct and quadrature currents. If I_q^{lim} is set as I_{max} it is the conventional one, characterized by setting the limits of the reactive current as the converter's maximum current capacity, which normally leads the active current reference to zero during a disturbance. The second one is to set $I_q^{lim} = \frac{I_{max}}{\sqrt{2}}$ and was proposed in the article [26]. Its characteristic is setting the reactive current limit at a value lower than the maximum capacity. As shown in the article the best limit's value is difficult to find as it depends on the grid configuration, so the value $\frac{I_{max}}{\sqrt{2}}$ was adopted as it is the same value adopted by the reference [26]. This change makes the reactive current assume $\frac{I_{max}}{\sqrt{2}}$ in case of saturation, thus the active power might assume a value different from zero, in this case, it will be also $\frac{I_{max}}{\sqrt{2}}$.

4.2.3 Control in $\alpha\beta$-Frame

The control in $\alpha\beta$-Frame is similar to the control in dq-Frame in concept, as it is based on a two-layer loop. The internal loop is shown in Figure 4.8, here a proportional resonant (PR) control is used. The PR works similarly to the PI but for sinusoidal quantities. The parameters are the same as the parameters for the control in dq-Frame as discussed in the Appendix A as presented in Table 4.9.

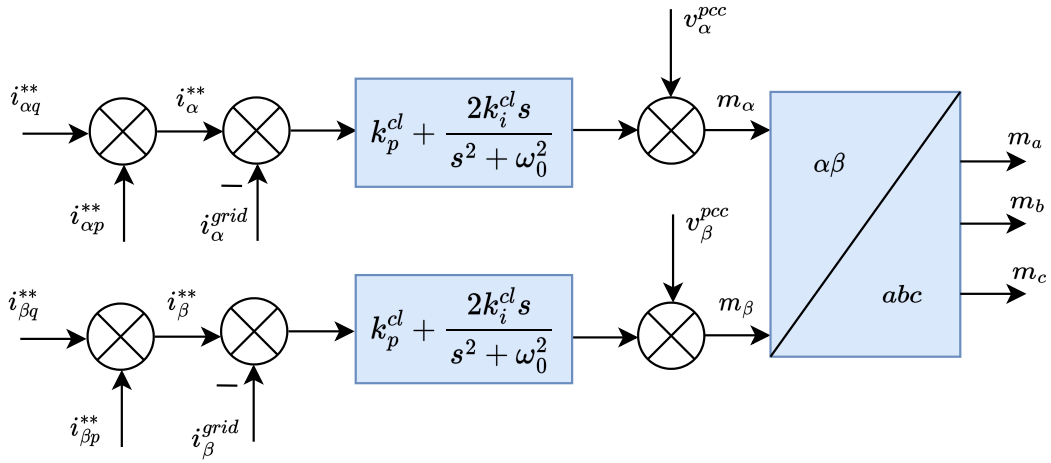

Figure 4.8: Inner loop control in $\alpha\beta$-Frame.

Table 4.9: Current loop parameters for the control in $\alpha\beta$-Frame.

Parameter	Value
k_p^{cl}	0.1449
k_i^{cl}	2.7214

Figure 4.9 shows the outer loop. It works in the same way as the control in dq-Frame, but the voltage and active power comparison results in reactive and active power references. To generate the current reference, it is used the reversed instantaneous power equation [43]. The currents responsible for generating the active and reactive power are generated separately in this loop to apply the current limit strategy discussed in [26]. The parameters are shown in Table 4.10.

Table 4.10: Outer loop parameters for the control in $\alpha\beta$-Frame.

Parameter	Value
$k_p^{apl-\alpha\beta}$	0.04
$k_i^{apl-\alpha\beta}$	5
$k_i^{vl-\alpha\beta}$	0.06
$k_i^{vl-\alpha\beta}$	15.625

The two ways of limiting the current magnitude adapted from the way discussed in [26] are presented in Figure 4.10.

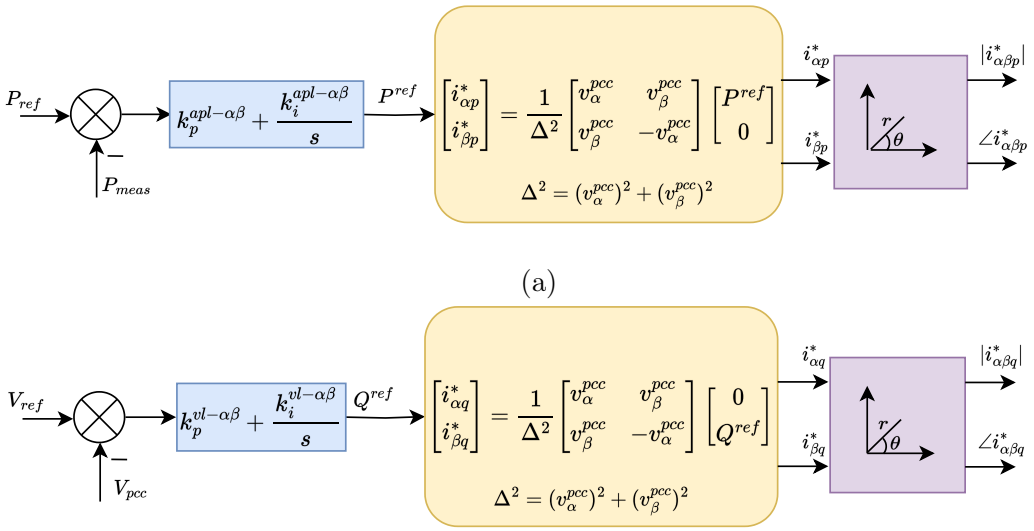

Figure 4.9: Outer loop control in $\alpha\beta$-Frame (a) active power outer loop and (b) reactive power outer loop.

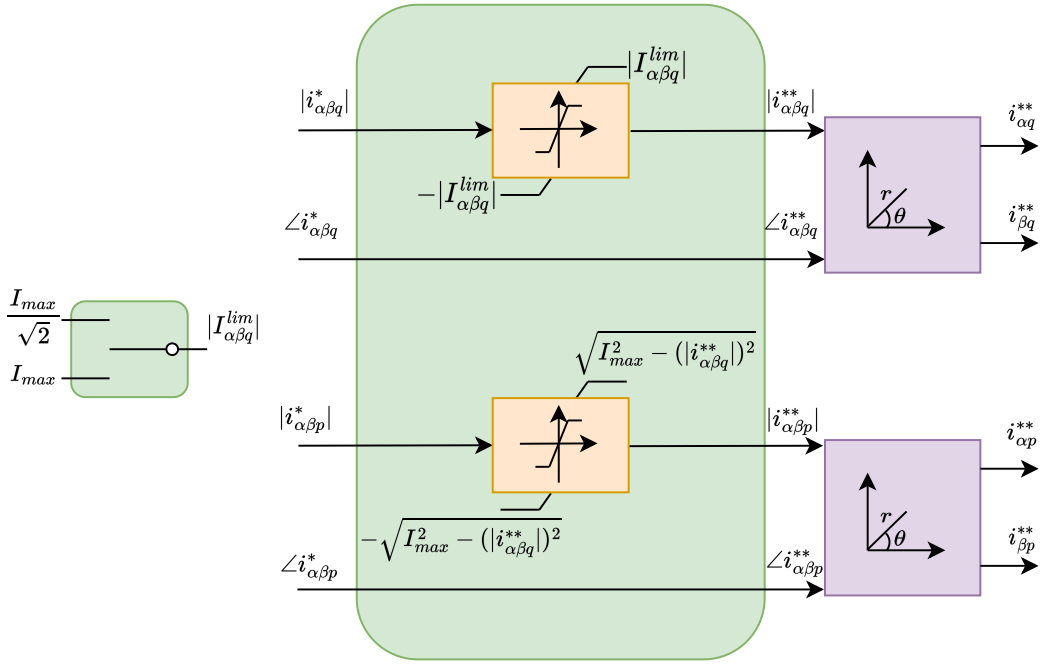

Figure 4.10: Current limiter based on the proposed in [26].

4.2.4 Synchonverter Control

The synchronverter is a control that aims to mimic the dynamic behavior of a synchronous machine, it was proposed in reference [6] and it is shown in Figure 4.11.

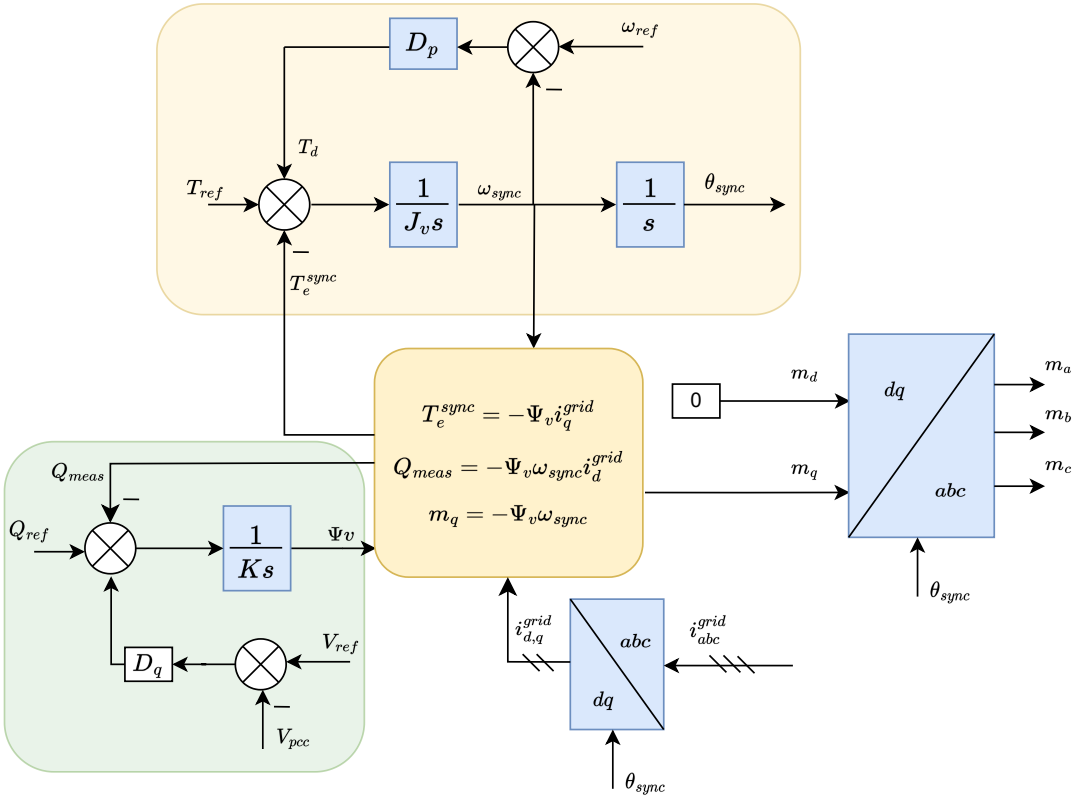

Figure 4.11: Conventional Synchronverter.

The synchronverter used in the comparative analysis is a modified version, shown in Figure 4.12 and the parameters used for the comparative analysis are shown in Table 4.11.

Table 4.11: Parameters for the adapted synchronverter.

Parameter	Value
D_{p1}	32
J_{v1}	2.5
R_{v1}	0.18
L_{v1}	0.9
$k_p^{vl-sync_1}$	0.5
$k_i^{vl-sync_1}$	20

To enable a fair comparison some changes were adopted in the synchronverter. First, the droop in the voltage loop control was removed and the integrator was changed to a PI. As the droop can reduce the voltage stability margin [27], as long

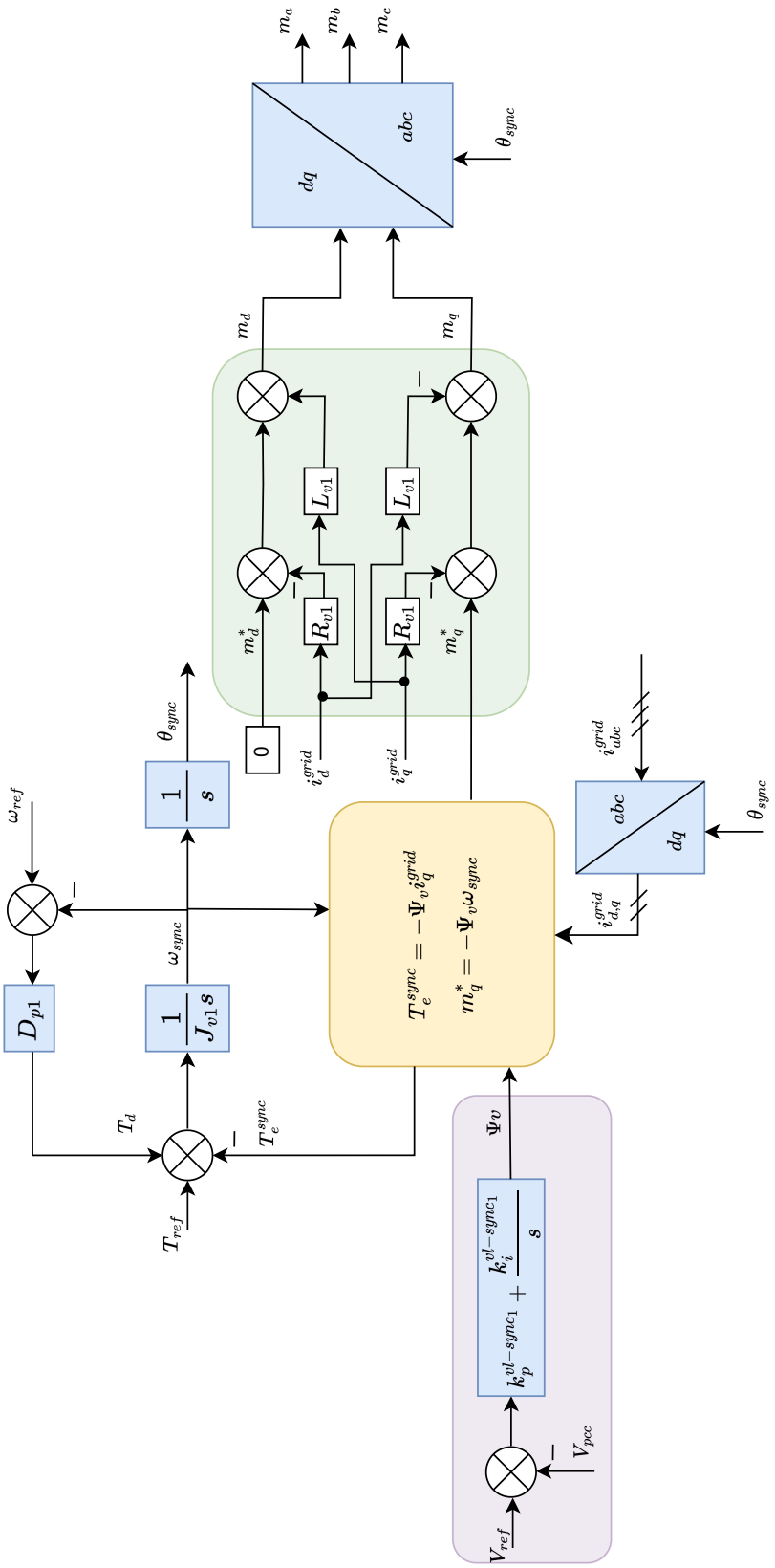

Figure 4.12: Synchronverter adapted for the comparative analysis.

as it acts to reduce the voltage reference in case of a disturbance. Moreover in the vectorial controllers presented in [40], there is no droop in the voltage loop and its controller is a PI, therefore in the synchronverter voltage loop, the controller was changed to a PI. Second, a virtual impedance is added to limit the current in the event of a short circuit, as described in [44]. It is worth mentioning that in a real case of multiple converters connected to the system, the droop control acts to avoid control interactions, therefore it is important to consider the droop control in future studies.

The synchronverter can be divided into three parts. The first part is shown in Figure 4.13 and it aims to mimic the mechanical equation of the synchronous machine.

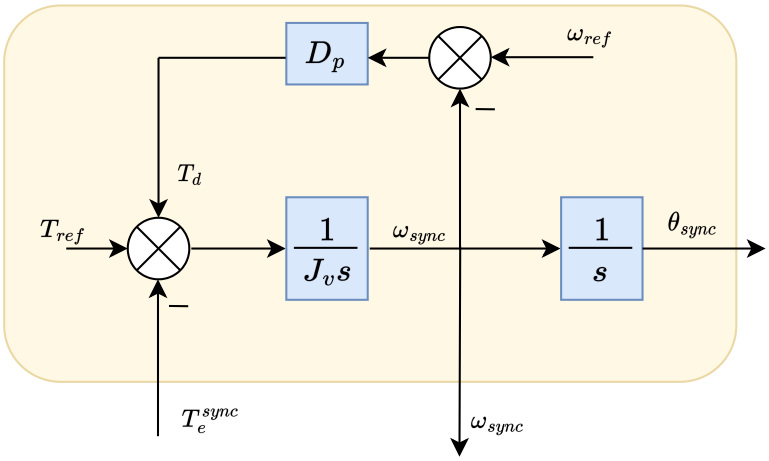

Figure 4.13: Mechanical equations.

The mechanical torque reference (T_{ref}), that in the synchronous machine comes from a turbine, in the synchronverter it is a controller reference equal to the active power reference in case the virtual speed (ω_{sync}) is equal to 1 pu, otherwise, the mechanical power reference is $P_{ref} = T_{ref} \times \omega_{sync}$. The virtual electromagnetic torque (T_e^{sync}) comes from the equations part of the synchronverter and it is added to the mechanical torque reference and the droop torque (T_d) with a minus sign. The droop torque, $T_d = D_p \cdot (\omega_{ref} - \omega_{sync})$, is responsible for the relationship between active power and frequency as in the conventional synchronous machine.

The torque summation represents the virtual acceleration of the machine that is integrated and divided by a constant, known as virtual inertia (J_v) generating the virtual speed (ω_{sync}), and after another integration, it generates the virtual angle (θ_{sync}).

The second part of the synchronverter is the voltage loop and it is shown in Figure 4.14. It is responsible for generating the virtual flux (ψ_v) as it implements the voltage-reactive relationship, besides, it controls the terminal voltage of the

synchronverter.

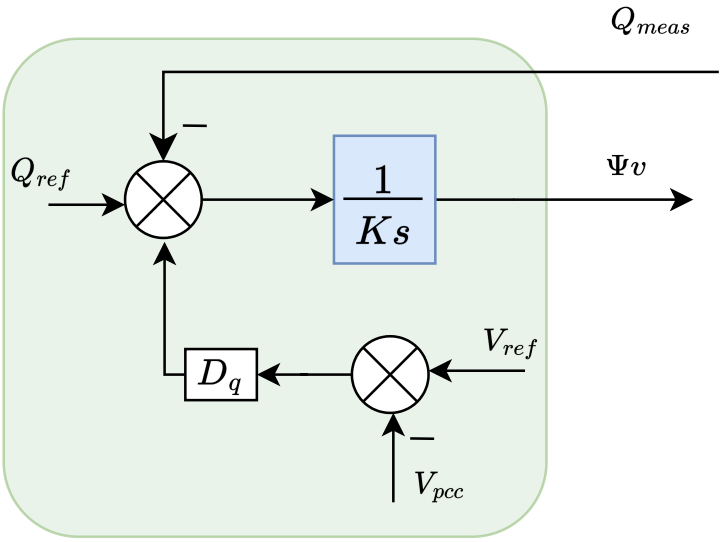

Figure 4.14: Voltage loop.

The third part of the synchronverter is shown in Figure 4.15. This par is responsible for calculating some variables needed in the other two parts of the synchronverter, it also generates the modulation index (m_q and m_d).

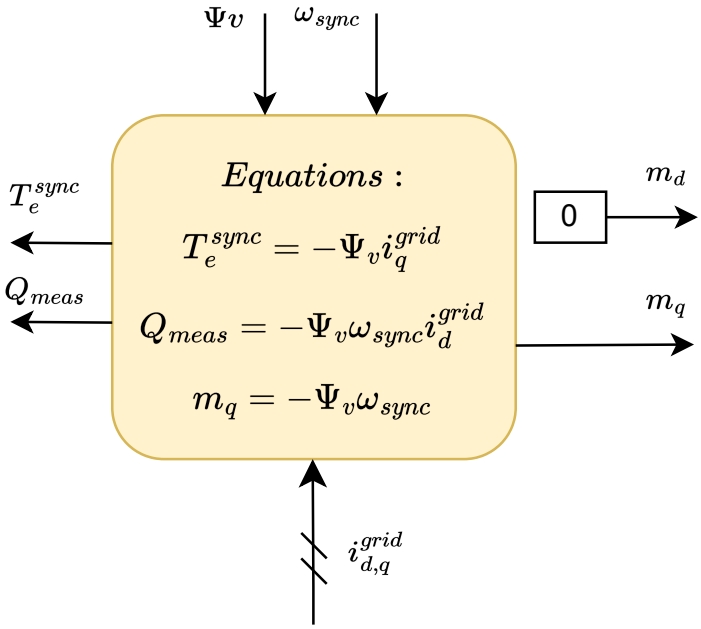

Figure 4.15: Equations.

4.3 Synchronous Machine Control

The synchronous machine model used in this dissertation was based on the ONS database [45]. The machine's AVR is shown in Figure 4.16, and its parameters are presented in Table 4.12. Although the over-excitation limiter was not included in the model from [45], it was added based on the model presented in [46] to enable more accurate analysis. The machine parameters are also shown in Table 4.13.

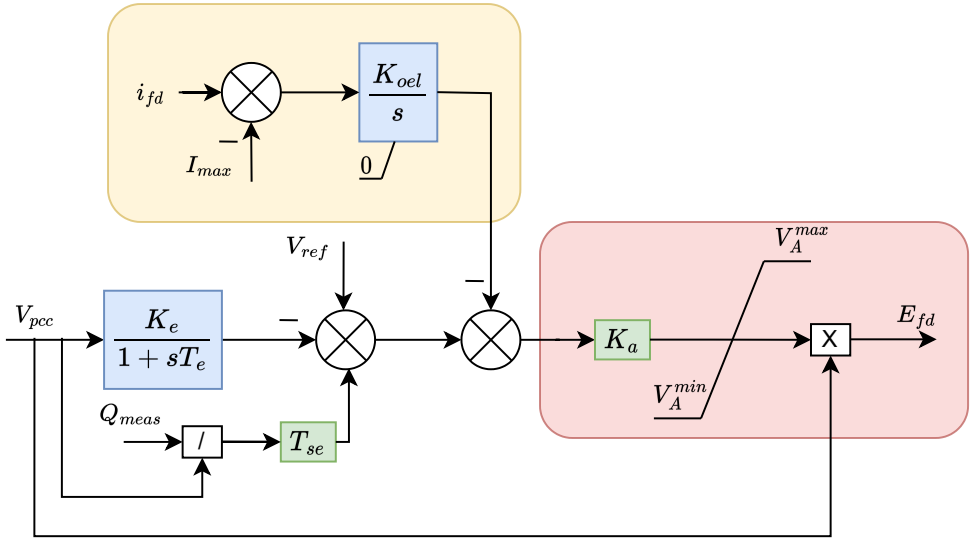

Figure 4.16: Synchronous machine AVR.

Table 4.12: Automatic Voltage Regulator parameters.

Parameter	**Value (pu)**
K_e	1
T_e	0.016
T_{se}	0.052
K_a	30.2
V_A^{max}	3.32
V_A^{min}	-3.75
K_{oel}	10
I_{max}	2.2

Table 4.13: Synchronous machine parameters.

Parameter	**Value**
V_{ll}	13.8 kV
I	2.803 kA
H	3.92 s
D	0
R_a	0.004 pu
x_p	0.075 pu
x_d	1 pu
x'_d	0.3 pu
T'_d	6.89 s
x''_d	0.22 pu
T''_d	0.04 s
x_q	0.68 pu
x''_q	0.22 pu
x''_d	0.22 pu
T''_q	0.11 s

Chapter 5

Methodology

5.1 Proposed Study

This dissertation aims to analyze three different cases:

- Comparative analysis between equipment regarding their influence on STVI;
- Sensitivity analysis of the rise time in the control in the dq-Frame about its impact on STVI;
- Analysis of the proposed change in the synchronverter virtual flux loop to improve its response in case of a short circuit.

Each case will be detailed in Section 5.1.1. For each case, three types of metrics will be measured, which are described in Section 5.1.2.

5.1.1 Studied Case

Comparative Analysis Between Equipment

This case study compares a synchronous machine and a power converter regarding their contribution to voltage stability in power systems. The power converter will be embedded with three types of control (Control in dq-Frame, Control in $\alpha\beta$-Frame, and, Synchonverter control) described in Section 4.2 which will also be compared with each other. The converters' control and AVR control performance design are described in Appendix A.

Sensitivity Analysis of Rise Time in the Control in dq-Frame

A sensitivity analysis will also be performed varying the rise time speed of the outer loop of the control in dq-Frame. This case aims to analyze whether the rise time speed influences the behavior under voltage instability and catch its influence. It is

worth mentioning that this study accounts for a single-infeed system, so it may be important to evaluate this case in a multi-infeed scenario [27, 28] for future research.

Change the Synchronverter to Enhance its Response in Case of Short-Circuit

A change in the synchronverter structure will be proposed for this dissertation based on references [26, 29].

Figure 5.1 shows the change proposed in the synchronverter adapted presented in Figure 4.12. During a short circuit, the synchronverter will change its virtual flux generation from voltage control to reactive power control. This change is proposed based on the fact that in a short circuit occasion, the voltage loop increases rapidly the virtual flux, so it also increases the reactive power in the system. In a limited power converter current capacity, all current capability would be located to reactive current, and as stated in [26], the system should inject active current along with the reactive current to improve its performance regarding STVI.

Therefore, this new structure makes it possible to control the power injection. The parameters for this analysis are shown in Table 5.1.

In this case study the proposed change in the synchronverter will be compared to the adapted one.

Table 5.1: Parameters for the synchronverter with the proposed virtual flux generator strategy.

Parameter	**Value**
D_{p2}	200
J_{v2}	0.1
R_{v2}	0.18
L_{v2}	0.9
$k_p^{vl-sync_2}$	0.5
$k_i^{vl-sync_2}$	20
$k_p^{rpl-sync_2}$	0
$k_i^{rpl-sync_2}$	20

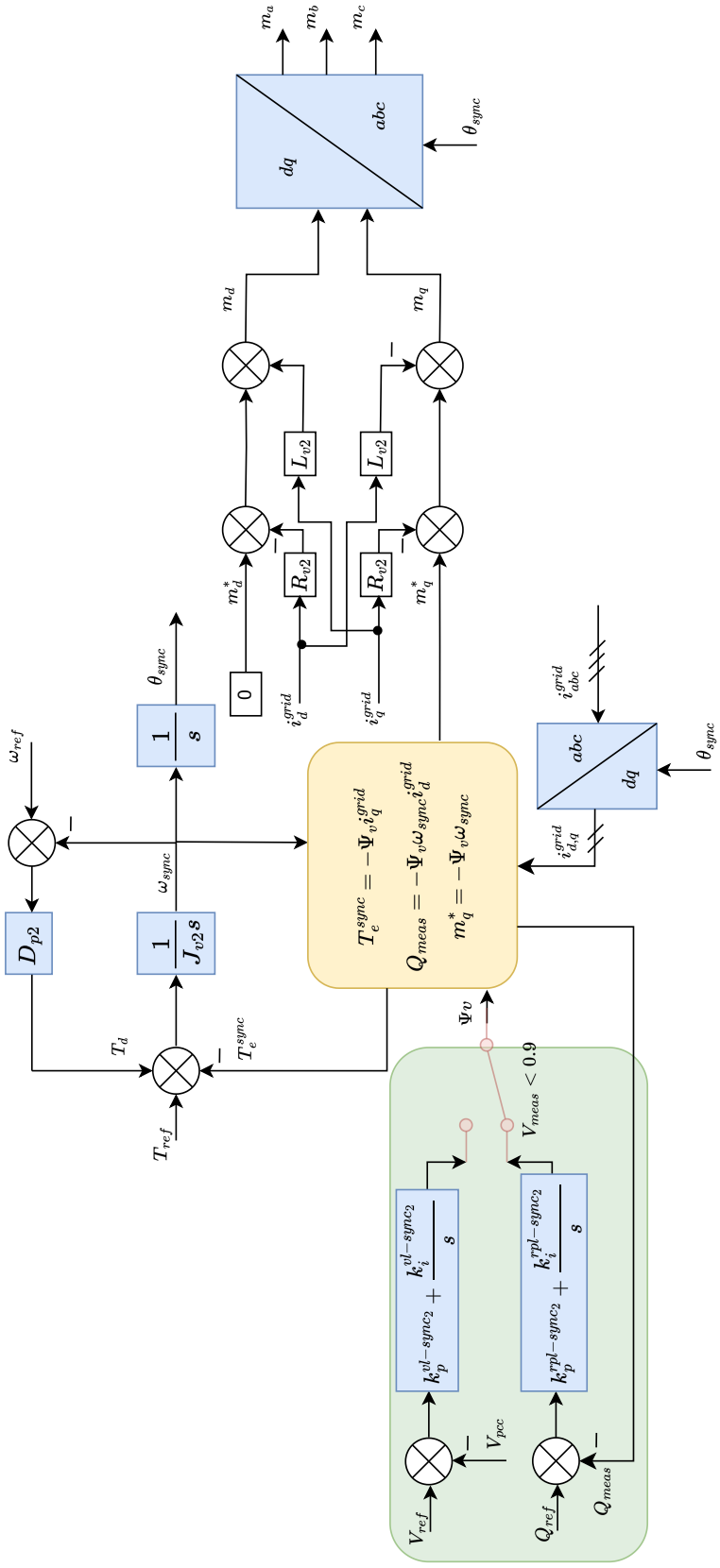

Figure 5.1: Proposed virtual flux generator for the synchronverter.

5.1.2 Analysis

Dynamic Behavior Under Short Circuit Analysis

This analysis is based on comparing the voltage recovery for a short circuit, by using the transient voltage stability ratio (TVSR). This metric was proposed in [25] and explained in Section 2.5. Figure 5.2 shows the system and the point of application of a short circuit.

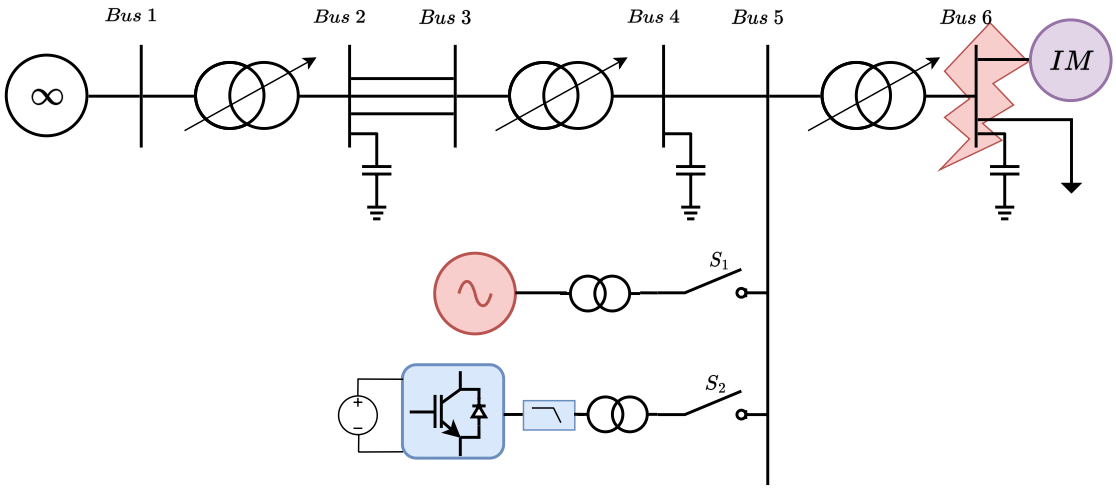

Figure 5.2: Short-circuit application.

Region of Attraction Limit Analysis

The region of attraction as explained in Section 3.1.2 is the largest set that the state vector can travel during a disturbance and keep being able to approach asymptotically a stable equilibrium point. For voltage stability analysis normally the region of attraction is measured by the biggest short-circuit duration that keeps the system stable [27]. In this dissertation study, the short circuit is applied at bus 6 for all analyses as shown in Figure 5.2. Figure 5.3 shows two cases of short circuits, it is possible to see that for 132 ms of short circuit the system is not able to recover stability, while for 131 ms the system recovers its stability, therefore, the CCT measured is 131 ms.

Saddle-Node Stability Margin Analysis

The saddle-node stability margin is a common voltage stability metric. In the literature, it is possible to find a lot of works that examine the distance of an operation point to the "nose" of a PV curve. But in this type of analysis, the static equations of the equipment are neglected, depending on the static equations of the load the bifurcation point might assume a different point as studied in reference [46].

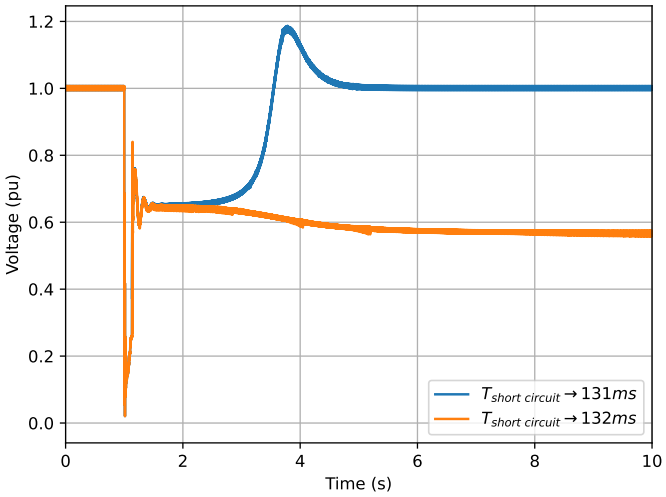

Figure 5.3: CCT measurement.

Therefore, this work proposes an analysis of the saddle-node stability margin which consists of an increase in the reactance that connects the power system to load slowly until the system collapses. The inductance variation is given by:

$$L = 0.002 \times t, \tag{5.1}$$

where, L is the inductance, and t is time.

The largest inductance obtained before a voltage collapse is the saddle-node margin. This analysis is shown in Figure 5.4.

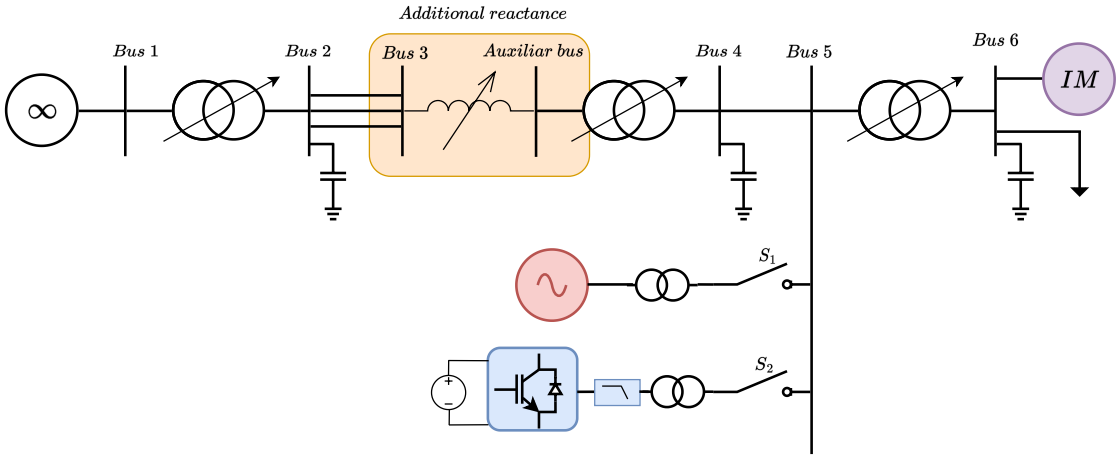

Figure 5.4: Saddle-node margin stability analysis.

Chapter 6

Results and Discussion

6.1 Equipment Comparison

This section intends to present the results of the comparative analysis between a synchronous machine and a power converter regarding its short-term voltage stability support. The result for the proposed analysis as presented in section 5.1.2 will be shown in each Section.

6.1.1 Dynamic Behavior Under Short Circuit

For this analysis, a short circuit for 70 ms was applied to bus 6, as shown in Figure 5.2. The voltage of bus 6 is shown in Figure 6.1, as can be seen, the dynamic response is different for each case and it is complicated to determine which one has a better result, as the vectorial controllers are faster to recover the voltage, but presents a large overshoot, while the machine and the synchronverter are slower but they do not present any overshoot.

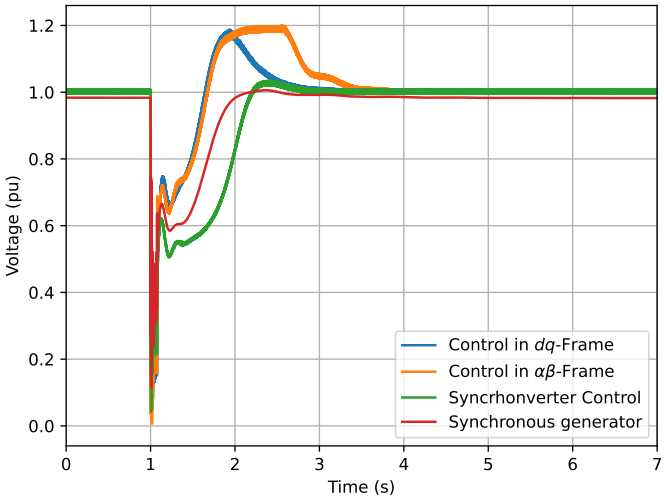

Figure 6.1: Voltage for 70 ms of short-circuit for different local generation.

Therefore, the analysis should be conducted based on a metric like the TVSR measured from each equipment's voltage response as shown in Figure 6.2.

The TVSR shows approximately the same value for the synchronous machine and the control in dq-Frame, 5.07% and 4.99% respectively. This happens because the metrics evaluate the area A_1 with the same weight as A_2. As their TVSR is lower than the TVSR for the synchronverter and the control in $\alpha\beta$-Frame, they present a better result.

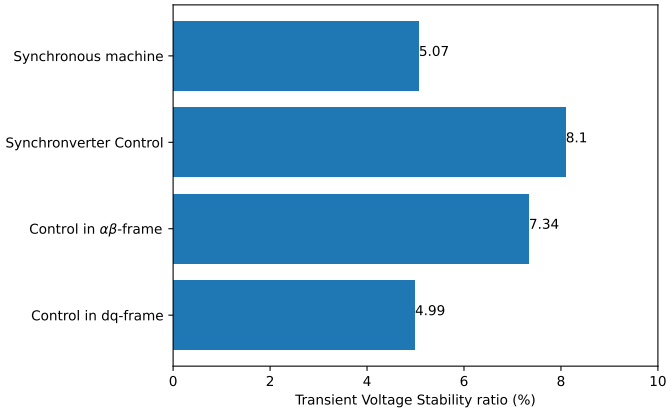

Figure 6.2: Transient Voltage Stability Ratio for different local generation.

The power converter has a limited current capacity, so it is important to analyze the current under short circuits. Figures 6.3a, 6.3b, 6.4a and 6.4b show the currents for the power converter with the three controls, and for the synchronous machine. The red line is the maximum allowable current for the power converter, in this case, 1.1 *pu*. As can be seen, the instantaneous current exceeds the maximum in some time instants. This operation will depend on the thermal limits of the converter, this analysis will not be done in this dissertation because this over-current is unexpected to interfere with the analysis.

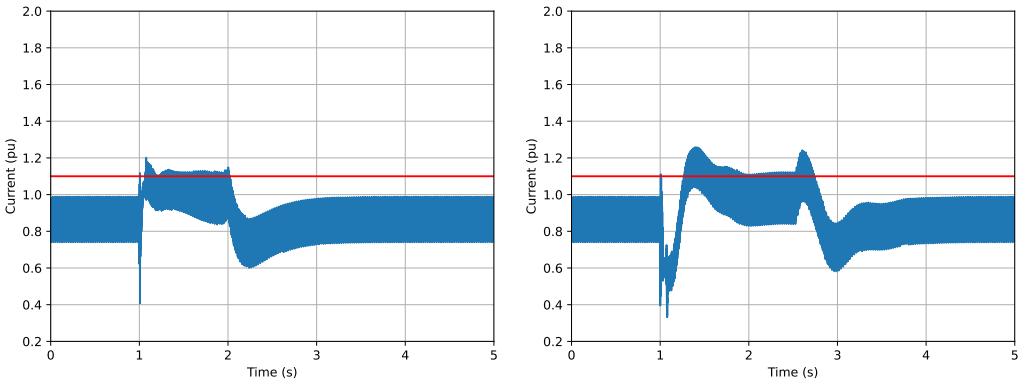

(a) (b)

Figure 6.3: Current analysis under short-circuit (a) Control in dq-Frame and (b) Control in $\alpha\beta$-Frame.

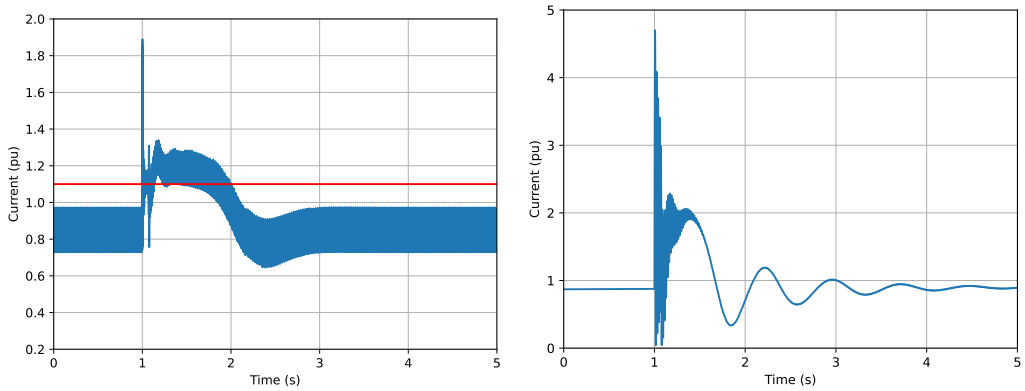

(a) (b)

Figure 6.4: Current analysis under short-circuit (a) synchonverter control and (b) synchronous machine.

For synchronous generators, the over-current capacity depends on the thermal characteristics of the generator's material and it will not be considered for this analysis. The behavior under the short circuit of the generator is shown in Figure 6.4b and will be considered acceptable, once the OEL is enabled.

6.1.2 Region of Attraction

Different durations of short-circuits were applied to the system as shown in Figure 5.2. The largest short-circuit duration known as CCT, which keeps the system stable for each case is shown in Figure 6.5.

The vectorial control (control in dq-Frame and control in $\alpha\beta$-Frame) presented the best result, while the synchronverter presented the worst. The synchronous machine shows an intermediate result, although its current capacity is much larger than that of a converter even for a short period.

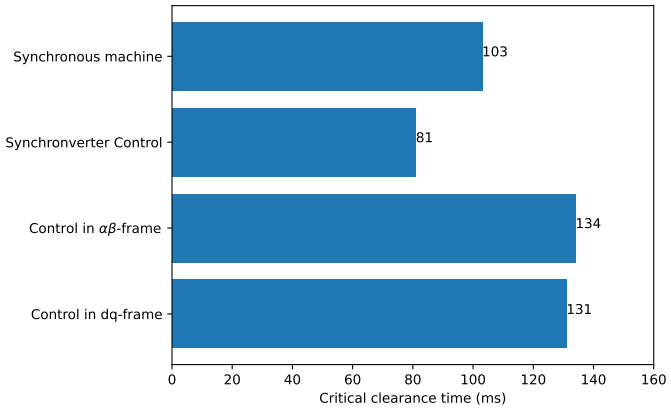

Figure 6.5: Critical clearance time for different local generation.

As can be seen in Figure 6.1, after a short circuit the vectorial controllers are

faster to recover the voltage than the synchronverter and the synchronous machine. This way, the voltage is higher for the system containing the vectorial control in the same instant during the disturbance, leading the induction motor to regain its capacity to re-accelerate. Therefore, the CCT is expected to be higher for the vectorial controller as confirmed in the analysis.

6.1.3 Saddle-Node Stability Limit

The saddle-node stability limit was evaluated as explained in Section 5.1.2. Figure 5.4 shows the system with an additional impedance. Figure 6.6 shows the voltage profile while increasing impedance.

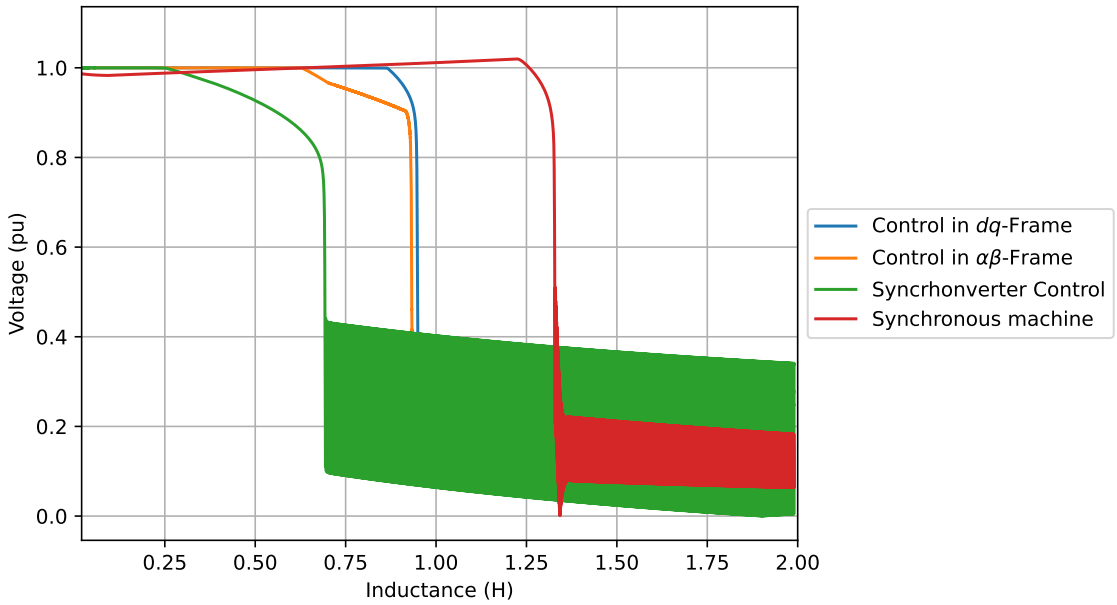

Figure 6.6: Saddle-node analysis for equipment comparison.

As can be seen, the synchronous machine got the best result as the voltage started falling with a larger reactance, but it is important to analyze the capability curve of the generator. The analysis is made in the long term, but the intention of the analysis is for the short-term dynamics and its stability. So, it is possible to conclude that the machine might not support this operation for a long time, but the short-term dynamics keep stable for a larger reactance than that for the power converter.

The synchronverter presents the worst result once it loses stability for the smallest reactance. Meanwhile, the vectorial controls (control in dq-Frame and control in $\alpha\beta$-Frame) present a similar response for an intermediate reactance.

The current contribution of each system under analysis is shown in Figure 6.7 and 6.8. In this case, the transient current is not analyzed, once this operation of continuous reactance increase is not normal. The analysis aims to measure the

largest reactance for which there is an equilibrium point. This equilibrium point might exist for a current above or lower than the rated. For a converter, this operation would be impossible, but for a machine, it depends on how much time the machine would operate under overload. However, in this dissertation, this analysis will not be addressed.

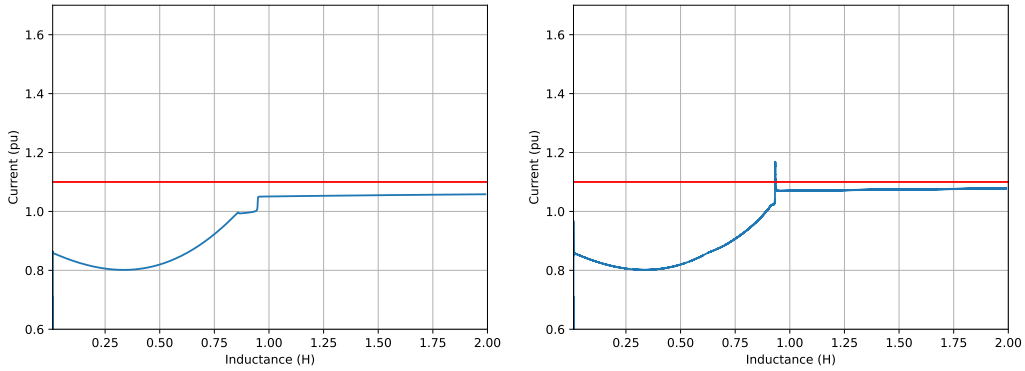

(a) (b)

Figure 6.7: Current analysis under reactance increase (a) control in dq-Frame and (b) control in $\alpha\beta$-Frame.

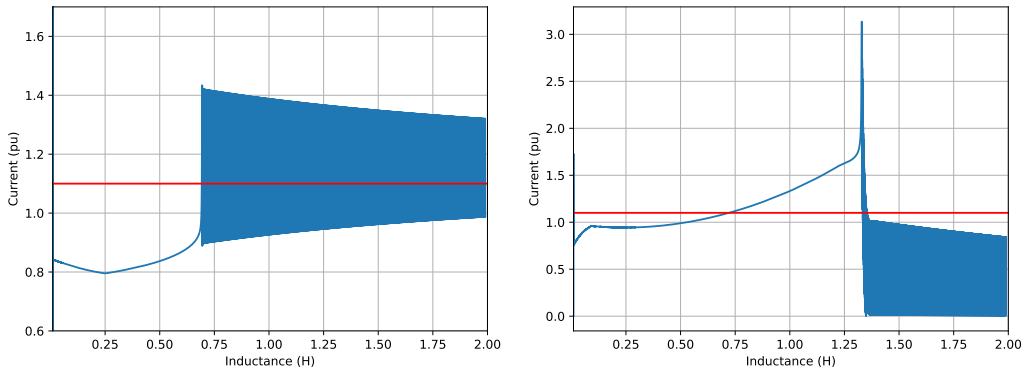

(a) (b)

Figure 6.8: Current analysis under reactance increase (a) synchronverter control and (b) synchronous machine.

6.2 Sensibility Analysis of Rise Time in the Outer Loop in the Control in dq-Frame

The rise time of the outer loop in the control in dq-Frame influence on the short-term voltage stability will be analyzed in this section. This analysis is performed in the article [29], and a difference in the impact of speed variation was found. There are some differences between the analysis in this dissertation and the article

mentioned earlier. First, the speed variation in the article [29] is made in the current loop instead of in the outer loop, second, the outer loop used in the article does not present any dynamic equation, it is composed of a division of the active and reactive power reference by the voltage to generate both reference currents. Thus, this section presents the analysis of the control in *dq*-Frame commonly used in the literature [40].

Tables 6.1 and 6.2 present the rise time for both the voltage and active loop and the corresponding outer loop PI parameters.

In the analysis of the influence of the active power loop rise time in STVI, the voltage loop rise time is kept constant as can be seen in 6.1, the same happens for the analysis of the active voltage loop rise time shown in Table 6.2, in this case, the active power loop rise time is kept constant.

Table 6.1: Parameters variation for the sensibility analysis of the active power loop in *dq*-Frame.

Voltage loop rise time	Active power loop rise time	k_p^{apl-dq}	k_i^{apl-dq}	k_p^{vl-dq}	k_i^{vl-dq}
1098.53	107.07	0.04	20	0.06103	15.2571
1098.53	221.03	0.04	10	0.06103	15.2571
1098.53	450.04	0.04	5	0.06103	15.2571

Table 6.2: Parameters variation for the sensibility analysis of the voltage loop in *dq*-Frame.

Voltage loop rise time	Active power loop rise time	k_p^{apl-dq}	k_i^{apl-dq}	k_p^{vl-dq}	k_i^{vl-dq}
60.92	221.03	0.04	10	0.06103	244.13
130.17	221.03	0.04	10	0.06103	122.06
268.73	221.03	0.04	10	0.06103	61.03
545.43	221.03	0.04	10	0.06103	30.51
1098.53	221.03	0.04	10	0.06103	15.26
2204.54	221.03	0.04	10	0.06103	7.63

6.2.1 Dynamic Behavior Under Short Circuit

Figure 6.9 displays the response to a short circuit varying the rise time for both outer loops. For the active power rise time variation shown in Figure 6.9a, there is no remarkable difference. But, for a variation in the voltage loop rise time, there are small differences in the voltage before its recovery and a notable difference in the overshoot as can be seen in Figure 6.9b. As slower the voltage loop is, the larger the overshoot is.

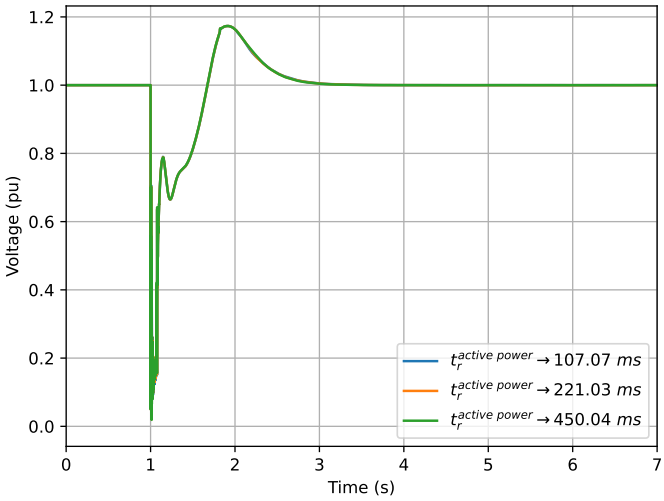

(a)

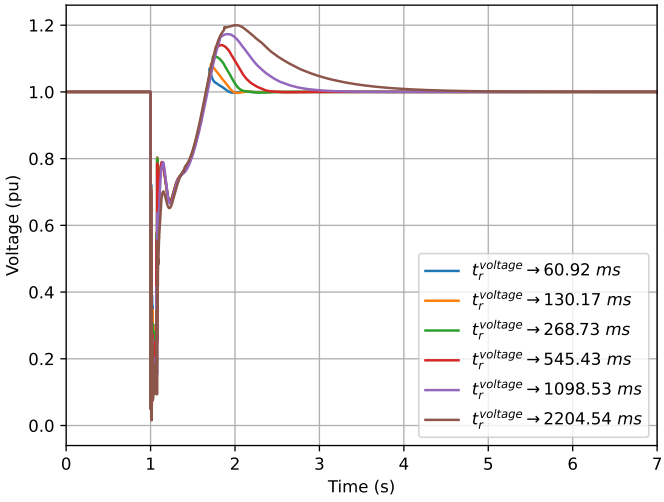

(b)

Figure 6.9: Voltage for a short circuit varying (a) active power rise time and (b) voltage rise time.

6.2.2 Region of Attraction

The region of attraction analysis is shown in Tables 6.3 and 6.4, respectively for the variation in the active outer loop and the variation in the voltage outer loop. There is no remarkable difference in the values the system loses voltage stability for the approximate same short circuit duration.

The voltage in the lower part, below the steady state value, presents the same dynamic as can be seen in Figure 6.9. Therefore, the induction motor liquid torque is approximately equal in any case. Thus, leading the system to have similar CCT values.

Table 6.3: CCT for active power loop rise time variation.

Active power loop Rise Time (ms)	**CCT (ms)**
107.07	131
221.03	131
450.04	131

Table 6.4: CCT for voltage loop rise time variation.

Voltage loop Rise Time (ms)	**CCT (ms)**
60.92	134
130.17	134
268.73	131
545.43	131
1098.53	131
2204.54	134

6.2.3 Saddle-Node Stability Limit

Figure 6.10 presents the saddle-node stability margin analysis for both rise time variations. As can be seen, there is no remarkable difference. Therefore, the rise time of the outer loop does not affect the saddle-node stability margin.

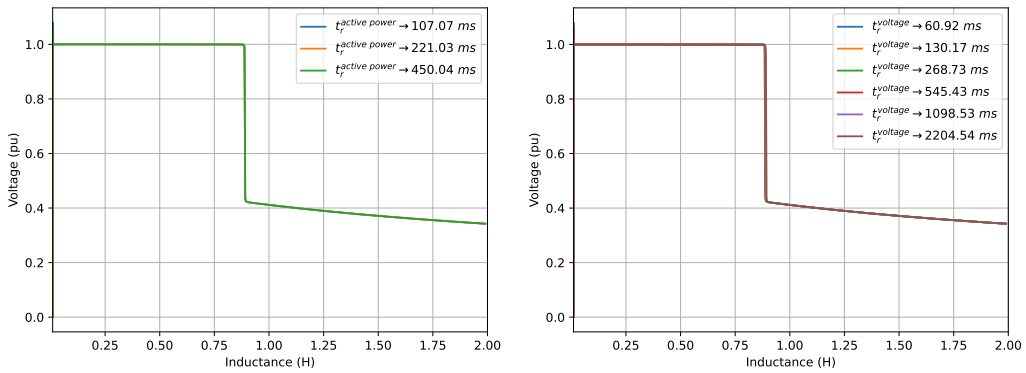

(a) (b)

Figure 6.10: Saddle-node analysis for (a) varying active power loop rise time and (b) varying voltage loop rise time.

6.3 Change in the Synchronverter Structure

A change in the synchronverter structure was proposed and explained in Section 5.1.1. This section shows the results of the analysis made to compare its performance with the adapted one.

6.3.1 Dynamic Behavior Under Short Circuit

Figure 6.11 shows the voltage for 70 ms of short-circuit duration for both, the adapted synchronverter and the proposed change in the virtual flux generation at Section 5.1.1. As can be seen in the voltage graph the proposed one shows better behavior in restoring the voltage and it can be measured by the TVSR as shown in Table 6.5.

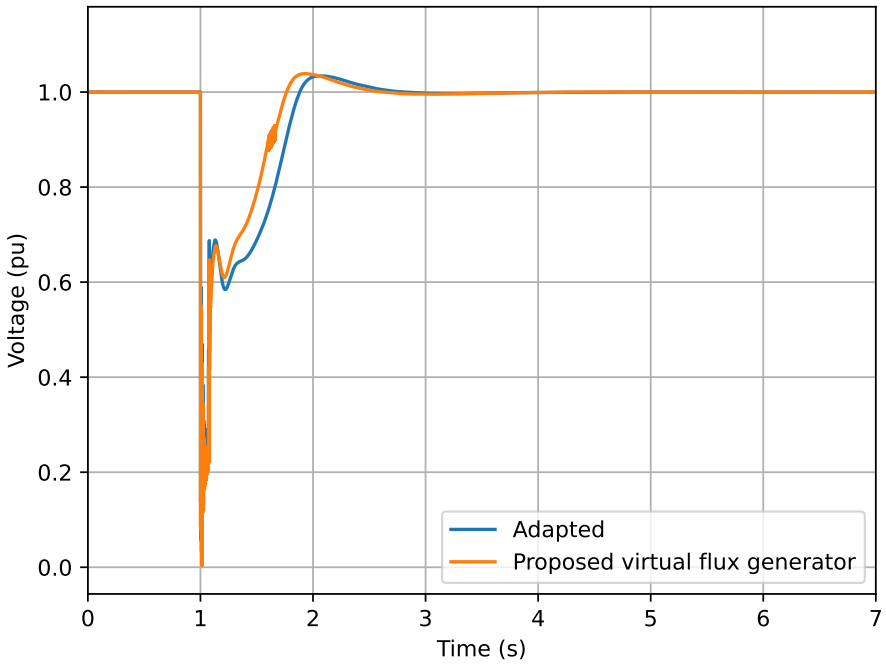

Figure 6.11: Short circuit comparison of the adapted synchronverter and the proposed one during 70 ms.

Table 6.5: TVSR for synchronverter.

Synchronverter	**TVSR (%)**
Adapted	4.746
Proposed	3.687

Figure 6.12 presents the current contribution of both synchronverters, the adapted one and the proposed one. As can be seen, both exceed the limit in some time instants.

6.3.2 Region of Attraction

The analysis for CCT is shown in Table 6.6. The proposed strategy for the virtual flux generation showed better resilience under short circuits, presenting a larger CCT than the adapted one.

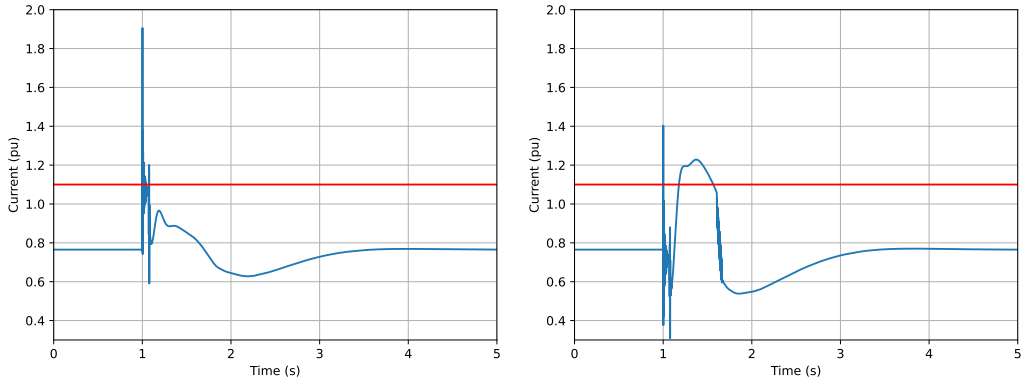

(a) (b)

Figure 6.12: Current for synchronverter (a) adapted topology Figure 4.12 and (b) proposed topology Figure 5.1.

Table 6.6: CCT for synchronverter.

Synchronverter	**CCT (ms)**
Adapted	120
Proposed	131

6.3.3 Saddle-Node Stability Limit

The saddle-node stability margin analysis was also performed. However, the results were not good, because the switch in the proposed virtual flux generation strategy led to instability when the voltage crosses the value of transition between the modes, 0.9 *pu*. From reactance zero until the reactance that leads the voltage to 0.9 *pu*, both show the same response as the control mode, and their parameters are the same.

Although this operation, increasing reactance, is not common in power systems, it is important to take providence to fix this issue, because this switch in the control when the voltage crosses the predetermined value, in this case, 0.9 *pu*, the synchronverter might lead the system to instability.

The currents for this operation are shown in Figure 6.14. As can be seen for the adapted one the current is always lower than the chosen limit.

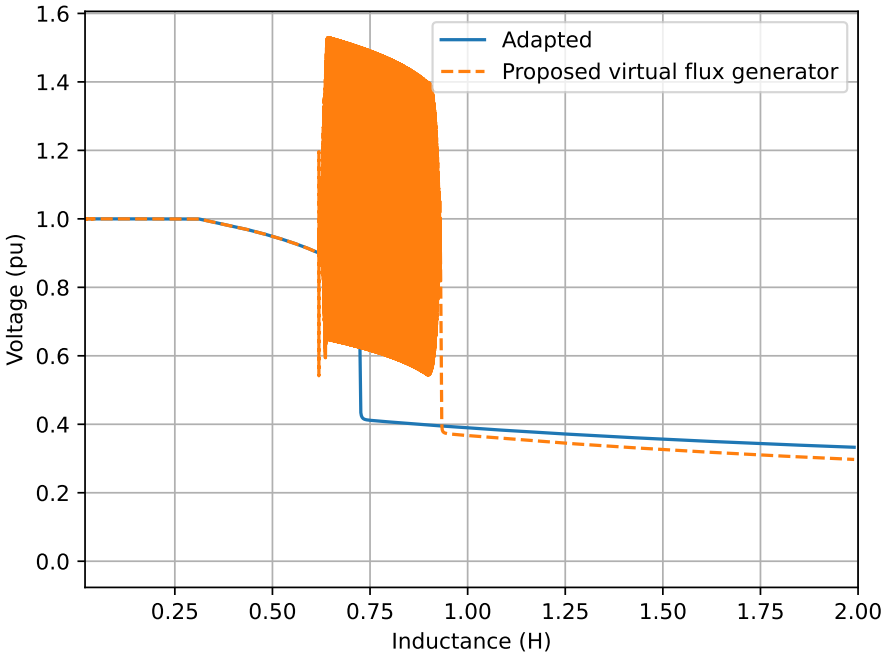

Figure 6.13: Saddle-node analysis for the adapted and conventional synchronverter.

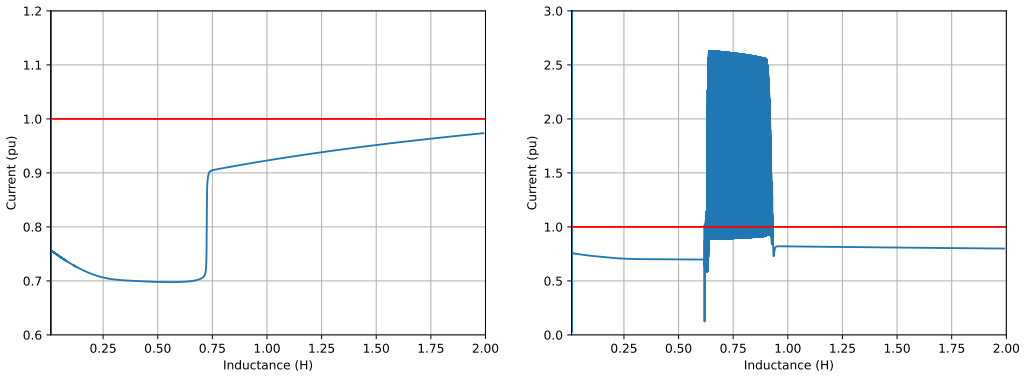

(a) (b)

Figure 6.14: Current analysis under reactance increase (a) adapted synchronverter and (b) proposed strategy for the virtual flux generation.

Chapter 7

Conclusions and Future Works

This work presented an analysis of how converters and their control affect short-term voltage stability. Furthermore, it presented a proposal on how to improve the voltage stability margin for the synchronverter by changing the virtual flux generator structure.

The bibliography review was presented at first, showing that there are few works related to short-term voltage instability and grid-tied converter, after that the theoretical foundations were presented, showing the mechanism of voltage instability based on dynamic system stability. The methodology proposed for the analysis was also presented and so the result was.

In the comparative analysis, a synchronous machine was compared to a converter with three control philosophies named: control in dq-Frame, control in $\alpha\beta$-Frame, and synchronverter. The dynamic behavior for a short circuit by using the transient voltage stability ratio [25] showed that the synchronous machine and the control in dq-Frame present a similar result and the synchronverter presents a similar result to the control in $\alpha\beta$-Frame. In terms of CCT, the synchronverter presented the worst result while the vectorial controls presented the best result. For the saddle-node stability analysis, the synchronverter presented the worst result and the synchronous generator the best.

An analysis of how the rise time of the outer loop of the control in dq-Frame affects STVI was also conducted, and the results showed that there is almost no difference, except that the overshoot after a voltage recovery is highly influenced by the voltage loop rise time. As faster the control is as lower the overshoot is, but in a real system with lots of power converters in the grid, more analysis of the interaction among them must be done.

A change in the synchronverter virtual flux generation based on the outer loop of the control in dq-Frame presented in references [26, 29] showed a promising result. The change showed an improvement in every metric analyzed, but an instability, when the voltage achieves the value that drives the mode to switch, might appear.

So, the synchronverter might be improved to give support to the grid in voltage instability cases.

7.1 Future Works

For future work, experimental validation might be done to prove the analysis of this dissertation. Analysis in scenarios with multiple converters connected to the grid is also important, once the controls might interact with each other [27, 28]. Moreover, include an impedance between the local generator and the bus to analyse its influence can be done.

The controllers used in this dissertation present only a positive sequence loop, so unbalanced short circuits were not tested. This way, the converters should also be compared in this case with negative sequence loops added to the control.

The third mechanism (Hopf bifurcation) was not tested in this dissertation and might be tested in future work to evaluate the performance difference between the converter and the machine.

The change proposed in the synchronverter in this dissertation showed promising results in terms of voltage stability improvement, but the switch in the virtual flux generator mode might lead the system to instability, this way the changes proposed here should be improved to avoid this.

References

[1] HATZIARGYRIOU, N., MILANOVIC, J., RAHMANN, C., et al. "Definition and classification of power system stability–revisited & extended", *IEEE Transactions on Power Systems*, v. 36, n. 4, pp. 3271–3281, 2020. doi: 10.1109/TPWRS.2020.3041774.

[2] EPE. "Plano Decenal de Expansão de Energia 2032". 2023. Disponível em: <https://www.epe.gov.br/pt/publicacoes-dados-abertos/publicacoes/plano-decenal-de-expansao-de-energia-2032>.

[3] ANEEL. "Banco de dados sistema de informações de geração da ANEEL". 2023. Disponível em: <https://dadosabertos.aneel.gov.br/dataset/siga-sistema-de-informacoes-de-geracao-da-aneel/resource/11ec447d-698d-4ab8-977f-b424d5deee6a>.

[4] ONS. "Previsões de carga para o Planejamento Anual da Carga 2023-2027", *Operador Nacional do Sistema Elétrico*, 2022.

[5] BORIČIĆ, A., TORRES, J. L. R., POPOV, M. "Comprehensive review of short-term voltage stability evaluation methods in modern power systems", *Energies*, v. 14, n. 14, pp. 4076, 2021. doi: doi.org/10.3390/en14144076.

[6] ZHONG, Q.-C., WEISS, G. "Synchronverters: Inverters that mimic synchronous generators", *IEEE transactions on industrial electronics*, v. 58, n. 4, pp. 1259–1267, 2010. doi: 10.1109/TIE.2010.2048839.

[7] KAWABE, K., TANAKA, K. "Analytical method for short-term voltage stability using the stability boundary in the PV plane", *IEEE Transactions on Power Systems*, v. 29, n. 6, pp. 3041–3047, 2014. doi: 10.1109/TPWRS.2014.2313152.

[8] VAN CUTSEM, T., GLAVIC, M., ROSEHART, W., et al. "Test systems for voltage stability studies", *IEEE Transactions on Power Systems*, v. 35, n. 5, pp. 4078–4087, 2020. doi: 10.1109/TPWRS.2020.2976834.

[9] BALU, C., MARATUKULAM, D. *Power system voltage stability*. McGraw-Hill New York, NY, USA, 1994.

[10] KUNDUR, P., PASERBA, J., AJJARAPU, V., et al. "Definition and classification of power system stability IEEE/CIGRE joint task force on stability terms and definitions", *IEEE Transactions on Power Systems*, v. 19, n. 3, pp. 1387–1401, 2004. doi: 10.1109/TPWRS.2004.825981.

[11] CIGRÈ. *Modelling of voltage collapse including dynamic phenomena*. Relatório técnico, Technical report of task force, 1992.

[12] G, M. D., M, S. J. *Use of Voltage Stability Assessment and Transient Stability Assessment Tools at PJM Interconnection*. Springer, 2021.

[13] AJJARAPU, V. *Computational techniques for voltage stability assessment and control*. Springer, 2007.

[14] ESO, N. "Technical report on the events of 9 August 2019", *Tech. Rep*, 2019.

[15] KAWABE, K., TANAKA, K. "Impact of dynamic behavior of photovoltaic power generation systems on short-term voltage stability", *IEEE Transactions on Power Systems*, v. 30, n. 6, pp. 3416–3424, 2015. doi: 10.1109/TPWRS.2015.2390649.

[16] VELOZA, O. P., SANTAMARIA, F. "Analysis of major blackouts from 2003 to 2015: Classification of incidents and review of main causes", *The Electricity Journal*, v. 29, n. 7, pp. 42–49, 2016. doi: doi.org/10.1016/j.tej.2016.08.006.

[17] BO, Z., SHAOJIE, O., JIANHUA, Z., et al. "An analysis of previous blackouts in the world: Lessons for Chinaś power industry", *Renewable and Sustainable Energy Reviews*, v. 42, pp. 1151–1163, 2015. doi: doi.org/10.1016/j.rser.2014.10.069.

[18] SANTOS, J. A. D. *Análise da estabilidade de tensão de curto prazo de sistemas de energia elétrica considerando a influência da desconexão mandatória de geradores síncronos distribuídos*. Tese de Doutorado, Universidade de São Paulo, 2020.

[19] SARAJCEV, P., KUNAC, A., PETROVIC, G., et al. "Artificial intelligence techniques for power system transient stability assessment", *Energies*, v. 15, n. 2, pp. 507, 2022. doi: doi.org/10.3390/en15020507.

[20] ONS. "System in numbers". 2023. Disponível em: <`https://www.ons.org.br/paginas/sobre-o-sin/o-sistema-em-numeros`>.

[21] ONS. “Requisitos técnicos mínimos para a conexão às instalações de transmissão, Procedimentos de Rede-Submódulo 2.10”. 2020.

[22] ONS. “Premissas, critérios e metodologia para estudos elétricos, Procedimentos de Rede-Submódulo 2.3”. 2020.

[23] DANISH, M. S. S., SENJYU, T., DANISH, S. M. S., et al. “A recap of voltage stability indices in the past three decades”, *Energies*, v. 12, n. 8, pp. 1544, 2019. doi: doi.org/10.3390/en12081544.

[24] WILDENHUES, S., RUEDA, J. L., ERLICH, I. “Optimal allocation and sizing of dynamic var sources using heuristic optimization”, *IEEE Transactions on Power Systems*, v. 30, n. 5, pp. 2538–2546, 2014. doi: 10.1109/TPWRS.2014.2361153.

[25] CABADAG, R. I. “Analysis of the impact of reactive power control on voltage stability in transmission power grids”, *PhD Thesis*, 2019.

[26] KAWABE, K., OTA, Y., YOKOYAMA, A., et al. “Novel dynamic voltage support capability of photovoltaic systems for improvement of short-term voltage stability in power systems”, *IEEE Transactions on Power Systems*, v. 32, n. 3, pp. 1796–1804, 2016. doi: 10.1109/TPWRS.2016.2592970.

[27] HUIJIE, C., WEN, H., CHAO, S., et al. “Transient voltage stability of paralleled synchronous and virtual synchronous generators with induction motor loads”, *IEEE Transactions on Smart Grid*, v. 12, n. 6, pp. 4983–4999, 2021. doi: 10.1109/TSG.2021.3104655.

[28] RAKIBUZZAMAN, S., ROBIN, P., MIKE, B. “The impact of voltage regulation of multi-infeed VSC-HVDC on power system stability”, *IEEE Transactions on Energy Conversion*, v. 33, n. 4, pp. 1614–1627, 2018. doi: 10.1109/TEC.2018.2831692.

[29] JALALI, A., ALDEEN, M. “Short-term voltage stability improvement via dynamic voltage support capability of ESS devices”, *IEEE Systems Journal*, v. 13, n. 4, pp. 4169–4180, 2018. doi: 10.1109/JSYST.2018.2882643.

[30] HOSSAIN, M. J., POTA, H. R., UGRINOVSKII, V. A., et al. “Voltage mode stabilisation in power systems with dynamic loads”, *International Journal of Electrical Power & Energy Systems*, v. 32, n. 9, pp. 911–920, 2010. doi: doi.org/10.1016/j.ijepes.2010.06.001.

[31] HOSSAIN, J., POTA, H. R. *Robust Control for Grid Voltage Stability: High Penetration of Renewable Energy: Interfacing Conventional and Renewable Power Generation Resources*. Springer, 2014.

[32] PSCAD. "Transient Analysis for PSCAD Power System Simulation–User's Guide", *Manitoba HVDC Research Centre*, 2002.

[33] VAN CUTSEM, T., VOURNAS, C. *Voltage stability of electric power systems*. Springer Science and Business Media, 2007.

[34] MONTEIRO, L. H. A. *Sistemas dinâmicos*. Editora Livraria da Física, 2019.

[35] STEVENSON JR, W., GRAINGER, J. *Power system analysis*. McGraw-Hill Education, 1994.

[36] MANNO, D. G., SEXAUER, J. M. *Use of Voltage Stability Assessment and Transient Stability Assessment Tools in Grid Operations*. Springer, 2021.

[37] KUNDUR, P. "Power System Stability and Control". 1994.

[38] FALCÃO, D. M., TARANTO, G. N. *Impact of the connections of large-scale wind and solar generation in the Brazilian interconnected*. e-papers, 2023.

[39] YONG, T., SHIYING, M., WUZHI, Z. "Mechanism research of short-term large-disturbance voltage stability". In: *2006 International Conference on Power System Technology*, pp. 1–5. IEEE, 2006. doi: 10.1109/ICPST.2006.321792.

[40] YAZDANI, A., IRAVANI, R. *Voltage-sourced converters in power systems: modeling, control, and applications*. John Wiley & Sons, 2010.

[41] ALVES, F., CASTAÑO, J. E. C., DE CASTRO, A. R., et al. "Projeto e aplicação de filtros lcl+ rc em inversores conectados à rede". In: *Congresso Brasileiro de Automática-CBA*, 2019.

[42] ROLIM, L. G. B., DA COSTA, D. R., AREDES, M. "Analysis and software implementation of a robust synchronizing PLL circuit based on the PQ theory", *IEEE Transactions on Industrial Electronics*, v. 53, n. 6, pp. 1919–1926, 2006. doi: 10.1109/TIE.2006.885483.

[43] AKAGI, H., WATANABE, E. H., AREDES, M. *Instantaneous power theory and applications to power conditioning*. John Wiley & Sons, 2017.

[44] R, H., K, M. M. “Analysis of Synchronverter Control with Virtual Impedance During Grid Voltage Variations”. In: *2021 IEEE 2nd International Conference on Smart Technologies for Power, Energy, and Control (STPEC)*, pp. 1–6. IEEE, 2021. doi: 10.1109/STPEC52385.2021.9718633.

[45] ONS. “ONS ANATEM DATABASE”. url:https://sintegre.ons.org.br/, fev. 2023.

[46] CORSI, S., TARANTO, G. N. “Voltage instability-the different shapes of the “Nose””. In: *2007 iREP Symposium-Bulk Power System Dynamics and Control-VII. Revitalizing Operational Reliability*, pp. 1–16. IEEE, 2007. doi: 10.1109/IREP.2007.4410582.

[47] ZMOOD, D. N., HOLMES, D. G. “Stationary frame current regulation of PWM inverters with zero steady-state error”, *IEEE Transactions on power electronics*, v. 18, n. 3, pp. 814–822, 2003. doi: 10.1109/TPEL.2003.810852.

[48] ALVES, F. A., TRICARICO, T. C., DE OLIVEIRA, D. S., et al. “A Procedure to Design Damping Virtual Impedance on Grid-Forming Voltage Source Converters with LCL Filters”, *Journal of Control, Automation, and Electrical Systems*, v. 33, n. 5, pp. 1519–1536, 2022. doi: doi.org/10.1007/s40313-022-00917-y.

Appendix A

Controllers Projects and Validation

A.1 Inner Loop Vectorial Controller Projects and Validation

The current loop for the dq-frame control in this dissertation was designed using the methodology described in [40]. By applying a modulus optimum and selecting a time constant within the range of [0.5, 5] ms, the PI parameters can be obtained in the form:

$$PI(s) = k_p^{cl} + \frac{k_i^{cl}}{s}, \tag{A.1}$$

in this case, the time constant was set to 4 ms. Figure A.1 shows the validation of the design for both axes, where it can be observed that the measured current matches the projected current.

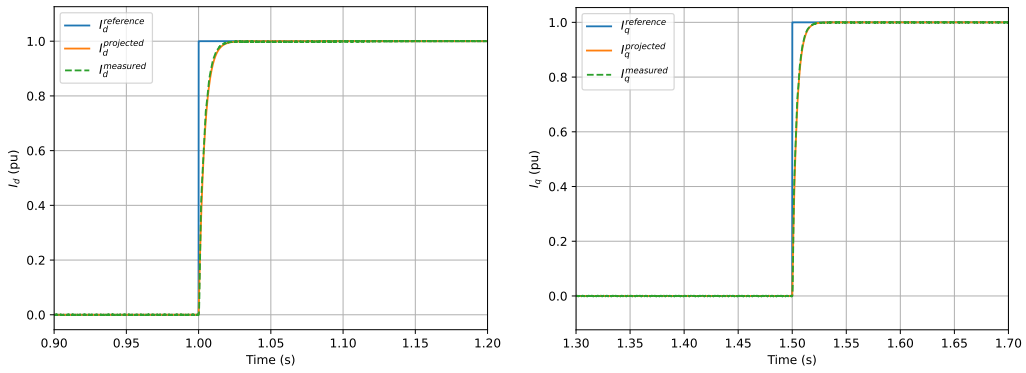

(a) (b)

Figure A.1: Inner loop in dq-Frame control validation (a) d-axis and (b) q-axis.

The control design in the $\alpha\beta$-Frame in this dissertation was based on the methodology outlined in [47]. The proportional resonant (PR) controller utilizes the same gains obtained for the PI controller in the dq-Frame and is given by:

$$PR(s) = k_p^{cl} + \frac{2k_i^{cl}s}{s^2 + \omega_0^2}, \tag{A.2}$$

where, k_p and k_i are the same parameters obtained for the control in dq-Frame, while ω_0 is the natural angular frequency of the system.

Figure A.2 illustrates the validation of the magnitude of the current vector, which is given by:

$$|I_{\alpha\beta}| = \sqrt{i_\alpha^2 + i_\beta^2}, \tag{A.3}$$

The measured value does not correspond to the projected one. As discussed in [48], different methods exist for projecting the PR controller. However, for this dissertation, the focus lies on achieving the same rise time for all equipment under analysis in the active power loop and voltage loop, as presented in Figure A.3 the rise time among the control strategies presents similar values. Therefore, the current loop project implemented is appropriate.

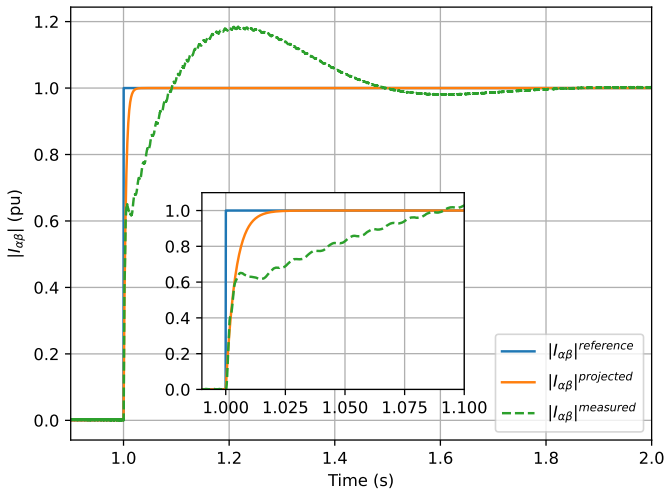

Figure A.2: Inner loop in $\alpha\beta$-Frame control validation

A.2 Voltage Loop Controller Project and Validation

The voltage loop control project was carried out through a trial and error process, using a reference of the rise time of 1100 ms. Figure A.3 displays the time response for a 0.05pu step change in the reference. In Table A.1, the measured rise time for all equipment is compared. The maximum relative error accepted is $\pm 5\%$, therefore, all the projects are considered suitable.

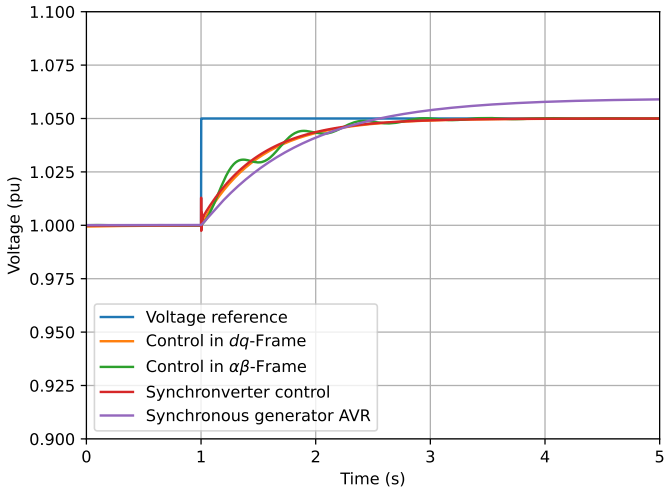

Figure A.3: Step response for 0.05 *pu* in the voltage reference.

Table A.1: Rise time comparison for voltage loop.

Equipment	**Rise time measured**	**Rise time reference**	**Error (%)**
Control in dq-Frame	1102.2	1100	-0.2
Control in $\alpha\beta$-Frame	1135.55	1100	-3.23
Synchronverter control	1095.15	1100	0.44
Synchronous machine AVR	1120.4	1100	-1.85

A.3 Active Power Loop Controller Project and Validation

The control loop for active power was also designed using a trial-and-error approach for all control strategies studied in this dissertation. However, the active power control for synchronous machines is typically slower than that for power converters, and in this study, a constant mechanical power model was used. Figure A.4 shows the step response for a reference of 0.8 *pu* in the active power reference. Table A.2 presents the measured rise time for each control loop and its comparison to the chosen reference of 220 *ms*. All the relative errors fall within the ±5% range, indicating that the results are acceptable.

Table A.2: Rise time comparison for active power loop.

Equipment	**Rise time measured**	**Rise time reference**	**Error (%)**
Control in dq-Frame	220.2	220	-0.091
Control in $\alpha\beta$-Frame	212.75	220	3.3
Synchronverter control	221.45	220	-0.66

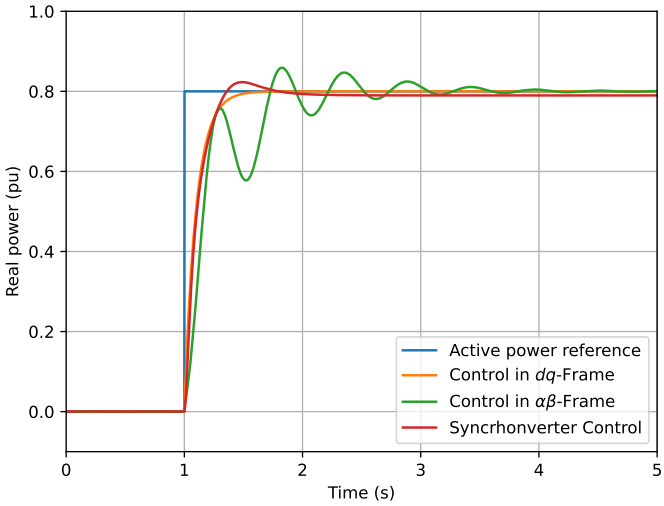

Figure A.4: Step response for 0.8 *pu* in the active power reference.